5-1994

Use of Multispectral Aerial Videography for Jurisdictional Delineation of Wetland Areas

James A. Shoemaker

USE OF MULTISPECTRAL AERIAL VIDEOGRAPHY FOR JURISDICTIONAL DELINEATION OF WETLAND AREAS

by

James A. Shoemaker

A thesis submitted in partial fulfillment
of the requirements for the degree

of

MASTER OF SCIENCE

in

Civil and Environmental Engineering

Approved:

UTAH STATE UNIVERSITY
Logan, Utah

1994

ACKNOWLEDGMENTS

I am thankful to Dr. Thomas Hardy for providing the opportunity to conduct this research. Without the investment of his time and his guidance, this project would not have come to such a successful end. I also am thankful to my committee members for their help in my understanding of critical areas of the project: Dr. Stevens for his statistical and mathematical insights, Dr. Neale for his system and knowledge of remote sensing, Dr. Gunderson for the guidance in fuzzy set theory and application, and finally, Dr. West for ensuring that as a non-biologist I didn't stray off the mark. I would thank my officemates, for without their help my hours of productive work on the computer would have been weeks of frustration.

Finally, I thank my wife, Shelly. Without her support and patience, none of this would have been possible.

James A. Shoemaker

CONTENTS

LIST OF TABLES

LIST OF FIGURES

ABSTRACT

Use of Multispectral Aerial Videography

for Jurisdictional Delineation

of Wetland Areas

by

James A. Shoemaker, Master of Science

Utah State University, 1994

Major Professor: Dr. Thomas B. Hardy
Department: Civil and Environmental Engineering

Multispectral aerial videography was used to reproduce the jurisdictional delineation of wetland area of approximately 50 hectares in Davis County, Utah. Imagery from the system consisted of three-band composite with wavelengths covering 550 nm (±10 nm), 650 nm (±10 nm), and 850 nm (±10 nm). The site was overflown at three different flight dates during the 1992 growing season (June 2, July 22, October 1). Imagery resolution varied from 0.56 m to 0.81 m. Mosaiced images were analyzed with a Supervised clustering/maximum likelihood classifier, ISODATA clustering/Euclidean classifier, statistical clustering/maximum likelihood classifier, and fuzzy c-means clustering. Overall accuracies for wetland/upland designation as compared to ground truth data varied from

60% to 75%. The ISODATA method was the poorest performer for all dates and both of two accuracy testing techniques. Supervised clustering and statistical clustering were comparable with a slight edge in accuracy to the supervised clustering. The best all-round performer was the fuzzy c-means algorithm in terms of time spent and accuracy. (123 pages)

INTRODUCTION

In 1972, the first of a series of Land Satellite (Landsat) remote sensing systems was launched. This system is unique in that it was the first system to provide "systematic, repetitive, observation of the earth's land areas" (Campbell, 1987, p. 6). This ushered in the era of easily accessible multispectral data for analysis of the earth's surface in digital form. This resource has helped managers in a number of fields including agriculture and natural resource management (Everitt, Escobar, and Nixon, 1987; Jackson, 1982; Lyon and Khuwaiter, 1988; Bukata et al., 1978; Bukata, Bruton, and Jerome, 1983; Bukata, Jerome, and Bruton, 1988; Kuchler and Zonnveld, 1988). Some researchers have also measured water quality in coastal and fresh water systems (Johnson and Harriss, 1980; Klemas et al., 1974; Lathrop and Lillesand, 1986; Lyon and Khuwaiter, 1988; Scherz and Domelen, 1975). Though the satellite systems provide useful data, there are some disadvantages inherent in their configuration. For example, with two Landsats in orbit, a geographic area is overflown only once every 9 days. Though the French imaging satellite SPOT increases this rate to once every 2 1/2 days through its pointable sensor array (Campbell, 1987), coverage is still hampered by cloud cover. Approximately 50% of the earth's surface is covered by clouds at any one time. This means that a Landsat overpass, on average, acquires a scene with only 1/8 of the sky obscured only twice a year (Rees, 1990).

Another problem is the necessary correction for atmospheric effects such as attenuation, scattering, and absorption (Rees, 1990). Strong absorption bands in the near-infrared (IR) range also restrict the use of sensors in this range. The altitude of a satellite also reduces the strength of the received signal by 200,000 times when compared to a platform at an altitude of 1 km. However, by far, the greatest problem is that of resolution. The pixel sizes of Landsat thematic mapper (30 meters) or SPOT (10 meters, panchromatic) imagery are too large to allow sufficient characterization of smaller features. The heterogeneity and small size of many natural features does not allow their monitoring using conventional satellite techniques.

Aerial-based videography presents a solution to the spatial resolution problem (0.25 to 3.0 meters per pixel) due to higher resolution sensors and its lower altitude of image acquisition. In addition, its rapid turnaround time (in comparison to satellite data acquisition) and ease of digitization (in comparison to higher resolution aerial photography) make it a useful data input for geographical information systems (GIS). The lower altitude also allows selection of monitoring frequencies that are absorbed by the upper atmosphere for use in plant species identification and determination of soil conditions (Everitt et al., 1987).

Researchers have developed a variety of single and multi-camera systems (Mausel et al., 1992). These systems have been successfully applied

in agricultural land-use classifications and assessments (Everitt et al., 1991; King and Vlcek, 1988; Marsh, Walsh, and Hutchinson, 1990), soil surface conditions (Everitt et al., 1988, 1989), determination of plant species (Blazquez, 1988; Everitt et al., 1987, 1988; Lulla et al., 1987; Nixon, Escobar, and Menges, 1985; Richardson, Menges, and Nixon, 1985), and natural resource management (Everitt, Escobar, and Nixon, 1987; Everitt and Nixon, 1985; King and Vlcek, 1990; Yuan, King, and Vlcek, 1991).

Wetlands

One area of interest to natural resource managers and engineers is the determination and monitoring of wetlands. To the lay person, a wetland can encompass a wide variety of qualitative descriptions: bog, marsh, swamp, mudflat. One researcher categorized 50 different terms in use to describe wetlands (Kusler, 1992). Part of the difficulty in precisely defining a wetland occurs because of its relationship as a transition zone between aquatic and terrestrial environments. In general, wetlands are "areas that are inundated or saturated by surface or ground water at a frequency and duration sufficient to support, and that under normal circumstances do support , a prevalence of vegetation typically adapted for life in saturated soil conditions" (Environmental Laboratory, 1987, p.13). These areas fulfill many functions such as floodwater storage and desynchronization, water quality improvement, erosion control, groundwater recharge, fish and

wildlife habitat, and heritage values (aesthetics, educational, recreation) (Grah and Crane, 1991; Want, 1989; Hook, 1986). Currently, only about 45% of the 221 million acres of wetland estimated to be present in 1780 remain in the conterminous United States (Want, 1989; Dahl and Johnson, 1991). Loss of these areas has led to a renewed interest in quantification of status, monitoring of trends, and protection of wetlands.

Legal History

The legislative history of wetlands in the U.S. began with the Rivers and Harbors Act of 1899, which gave the U.S. Army Corps of Engineers (Corps) approval authority for obstructions in navigable waters. This role has expanded to the current Clean Water Act Section 404, giving the Corps responsibility, subject to Environmental Protection Agency review, to regulate the discharge and fill of material into wetland areas (Want, 1989). In order to fulfill this responsibility, the Corps permit process requires that the boundaries of wetland areas be determined. The size of the area (e.g., 1 acre [0.40 hectare] versus 10 acres [4.04 hectares]) has a dramatic effect on the regulatory framework the permit process takes (Want, 1989). The National Wetland Inventory (NWI) maps produced at 1:24000 do not have sufficient spatial resolution to meet the Corps 1:6000 mapping requirements. A recent study of Corps-issued permits in Oregon (January 1977 through January 1987) and Washington (1980-1986) indicated that

66% (Oregon) and 65% (Washington) of the impacted areas were less than one acre in size (Kentula et al., 1992). This interest in wetlands both from the permitting process and other legal and institutional considerations has led to attempts by some agencies to determine the presence and extent of wetland areas within their jurisdiction or under their management or regulatory purview. For example, the state of Washington Department of Transportation (WDOT) has begun an effort to inventory wetlands along highway rights-of-way (Ossinger, Schafer, and Cihon, 1992).

Remote Sensing Efforts

Previous researchers have used a variety of remote sensing techniques to quantify and examine wetlands. Bartlett and Klemas (1980) examined Landsat/multispectral scanner (MSS) data and found it suitable for estimating biomass in mid-Atlantic tidal wetlands. Dottavio and Dottavio (1984) compared simulated Landsat/MSS and Landsat/Thematic Mapper (TM) data for broad community identification. In discriminating between agriculture, upland forest, brackish high marsh, brackish low marsh, and water classes, overall classification accuracies of 65.6% (MSS) and 69.4% (TM) were obtained. Another group of researchers used Landsat/TM to classify a portion of Maryland's Eastern Shore bordering the Chesapeake Bay into forest, agriculture/grass, water, and wetlands with an 81% accuracy (Ormsby et al., 1985).

Data from the Landsat used to classify coastal wetlands in South Carolina resulted in accuracies of 86.7 to 92.3% (Jensen et al., 1993a). The Environmental Protection Agency evaluated both Landsat and aircraft-based MSS for wetland identification in southwestern Florida. Accuracies were 68% for aircraft MSS (7.6 m resolution) and 74% for Landsat/MSS (Butera, 1979). Jensen and others have done extensive work in the area of remote sensing of wetlands in South Carolina. A 1981 study using an aircraft MSS (3 m resolution) resulted in 83% accuracy for wetland classification (Jensen et al., 1986). A follow-on study with multiple flight dates with an aircraft MSS (5.6 m resolution) found 82-86% accuracy (Jensen et al., 1987).

Probably the most commonly used method to remotely identify wetlands is aerial photography (Mitsch and Gosselink, 1986). Recent uses include a pilot study by WDOT using color and color-IR photography at a variety of scales to delineate wetlands with areas as small as 0.25 acres. Though no accuracies were reported, the color-IR photos at 1:12000 gave acceptable classification results (Ossinger, Schafer, and Cihon, 1992). An investigation of techniques for this project included a live demonstration of a videography system that was not used in any formal data analysis. In 1975 the U.S. Department of the Interior Fish and Wildlife Service began a project to inventory wetlands in the United States to aid managers in the wise use of this resource (Tiner, 1990). This project, the National Wetlands

Inventory (NWI), makes use of high altitude aerial black and white photography at 1:80000 and color infrared photography at 1:56000 scales, giving a feature resolution of 1-3 acres.

These various efforts generated classifications with typical overall accuracies of 60-90% at scale resolutions of 3-30 meters. Though the classification accuracies are acceptable, the resolution is generally still not sufficient to meet the Corps mapping requirements. National map standards require that no more than 10% of the points on a map with scale larger than 1:20000 can have a horizontal position error of more than 0.8 mm (1/30 in.). For the 1:6000 Corps requirements, this 10% accuracy limit is 4.8 m. For normal vision, plotting accuracies of 0.25 mm to 0.5 mm (1/100 to 1/50 in.) can be resolved, which translates to positional accuracy of 1.5 m to 3 m (4 to 6 ft) (Wolf and Brinker, 1989). Thus other methods are required to produce wetland classifications at a scale that will meet requirements for Corps jurisdictional delineation.

With greater spatial resolution than satellites and lower cost in comparison to aerial photography, multispectral videography offers the possibility to meet these mapping requirements. Though aerial photography can offer greater spatial resolution, its lack of automated processing capability hampers its use for larger projects. Also, its combined spectral information requires extensive processing to obtain the separate spectral information that is readily available from the multispectral

imagery. The possible problems from film developing errors (temperature variability, exposure time, chemical variation) can alter the final film appearance and so alter the spectral information obtainable from the print. Multispectral videography eliminates these shortcomings because its data are collected in the more stable and repeatable medium of digital videotapes. Another system that would overcome the shortcomings of aerial photography is aircraft MSS. However, the high cost of its specialized equipment in comparison to the relatively inexpensive price of the mass market commercial equipment used in the multispectral system makes it uneconomical for routine use. In summary, the digital nature, repeatability, and relative inexpensiveness of multispectral video data make it easily subject to computerized processing of its spectral information, and the relatively low cost makes it amenable to routine use. The literature reports no efforts to perform jurisdictional delineations of wetlands using a remotely sensed approach.

This study investigated the use of multispectral videography in jurisdictional delineation of a known wetland area. The test site was delineated the summer previous to the overflights as part of the Corps permitting process and the data from this jurisdictional delineation were used as ground truth for accuracy assessment (Grah and Crane, 1991). The first objective was to compare results of wetland classification using supervised and unsupervised classical spectral clustering as well as

maximum membership fuzzy c-means clustering from imagery collected with an airborne multispectral videography system. Second, the temporal effects on classification arising from seasonal variations of three different flight dates were inspected. Finally, all the information was examined to determine the suitability for use of multispectral videography in jurisdictional wetland delineation.

MATERIALS AND METHODS

Site Description

The wetland investigated is located south of Farmington, Utah just east of the Great Salt Lake (Sec 13 & 14, T3N R1W in Davis County, Utah) (Grah and Crane, 1991) (see Figure 1). Multispectral imagery were acquired on June 2, July 22, and October 1, 1992, using the multispectral videography system described below with spatial resolutions of 0.69 m, 0.81 m, and 0.56 m for each date, respectively. A subset of the jurisdictionally delineated site was selected as the test area. Though the delineation for this site was completed in June 1991, under existing Corps regulations jurisdictional delineations are valid for 2 years (Want, 1989) so that this delineation (Grah and Crane, 1991) was considered valid for use as ground truth.

Data Acquisition

The aerial multispectral videography system used for data collection was developed at Utah State University (Neale, 1992). This system consists of the following items: (1) three COHU 4810 series high resolution (525 horizontal lines) monochrome CCD video cameras with 10-nm interference filters centered on 550 nm (green), 650 nm (red), and 850 nm (infrared) and

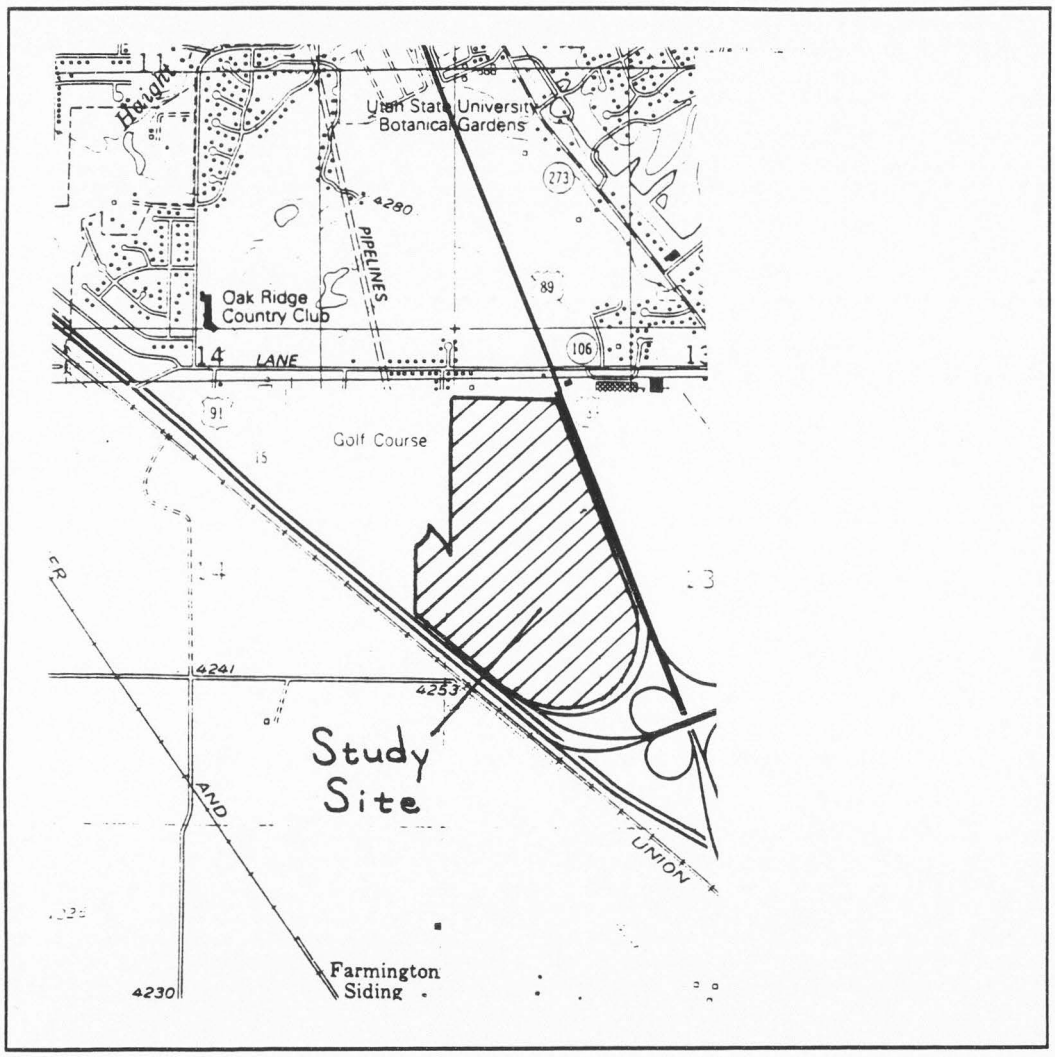

Figure 1. Site location in Utah.

with a 16-mm Sony television quality lens; (2) three Panasonic AG-7400 S-VHS videotape recorders (425 horizontal lines) for recording camera output; (3) an Exotech four-band radiometer with Landsat Thematic Mapper bands TM1 (450-520 nm), TM2 (520-620 nm), TM3 (630-690 nm), and TM4 (760-900 nm) with square 1-degree field-of-view lens; (4) an Everest thermal infrared radiometer (8-14 μm) with a circular 2-degree field-of-view; (5) an Omnidata 700 series Polycorder datalogger for recording dc camera voltages and analog signals from the two radiometers; (6) a Trimble Pathfinder global positioning system (GPS) with output recorded by an Omnidata 600 series datalogger; (7) a SMPTE time code generator to provide time/frame counts for image digitization at a later time.

The cameras and radiometers were mounted in a vibration isolation frame to minimize blurring. Camera lens focuses were set at infinity and the focal axes aligned to converge on an object at the expected height above ground for data collection. All three cameras were synchronized with the green camera designated as the master, thus allowing all three cameras to simultaneously record the same image. The synchronization signal from the master camera was fed to the time code generator to supply time/frame code information which was recorded on audio channel #2 by each videorecorder. The time/frame code information was also provided in a data block on the bottom of the green camera image for visual reference during image

digitizing. Another data block on the bottom of the red camera image contained GPS information from the Trimble Pathfinder.

Image Preprocessing

Images were viewed and digitized with a Panasonic S-VHS AG-7500 editing machine controlled via a Diaquest board and software system on a PC-386 (Neale, 1992). The Diaquest board used the time code to locate the same scene on each monochrome videotape for automatic digitization of desired frame sequences. Individual frames were digitized to an 8-bit (256 gray scales) file using a TARGA+ board for transfer and processing on an IBM RS-6000 530H workstation. Data processing on the workstation was conducted using the Earth Resource Data Analysis System (ERDAS) and software developed for this project.

Images were first corrected for vignetting via procedures established by Crowther (1992) and Crowther and Neale (1991). Vignetting is the darkening of the image with increasing distance from the center of the lens. The vignetting correction adjusts the imagery for departures from perfect focusing, which causes this effect, as well as accounting for nonuniformities in the camera sensing chip. Three-band false color composite images of each video scene were constructed by registration of the red and infrared images to the green image (see Figure 2). The interlaced scanning resulting from the RS-170 television standard resulted in a horizontal shifting due to

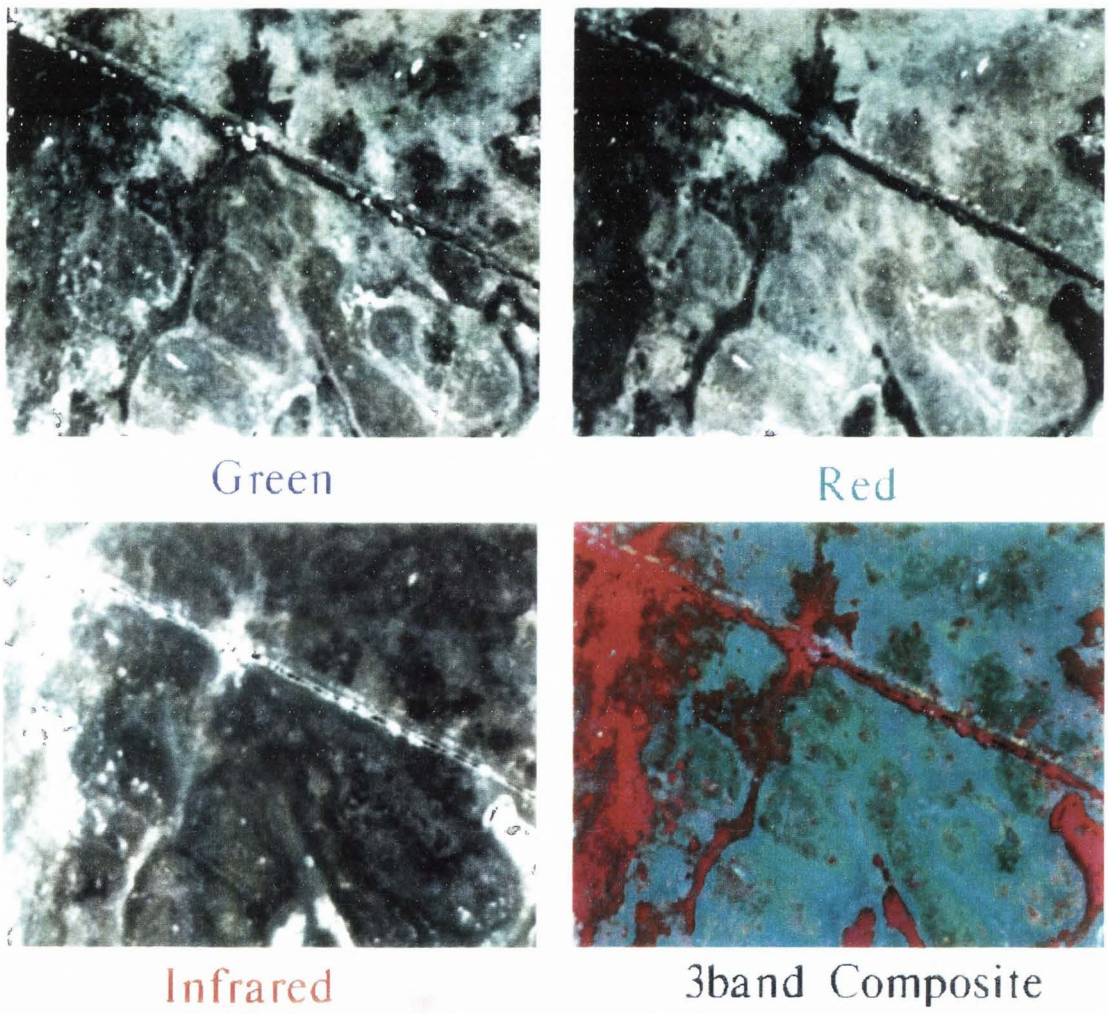

Figure 2. Example single bands and 3-band false color composite.

aircraft motion perpendicular to the flight path (transitional and roll effects) and a vertical shifting due to both forward plane motion and pitch. Image shifts due to platform yaw were not corrected. Vertical line shifting was corrected by maximizing the correlation of the summed brightness values for shifting of odd/even lines (Neale et al., 1993). Every tenth value in an image-centered window 1/9th the size of the image was used in the correlation. Horizontal line shifting was then performed in the same manner. Images were then visually reviewed to confirm the selected shifting. These 3-band composites for each flight (June - 32 images, July - 17 images, October - 29 images) were stitched into a mosaic for analysis and presentation purposes (see Figures 3-5).

The individual 3-band images were clustered and classified using three classical techniques: (1) supervised clustering with a Bayesian/ maximum likelihood classification; (2) iterative self-organizing data analysis technique (ISODATA) which used a Euclidian distance classifier; and (3) statistical clustering with a Bayesian/maximum likelihood classification (ERDAS, 1991). The stitched images were also evaluated using a fuzzy c-means pattern recognition algorithm (Gunderson and Jacobsen, 1983).

The classical signature evaluation and classification was performed with the ERDAS software package on an IBM RS/6000 Model 530H.

Figure 3. June 2, 1992 mosaic image.

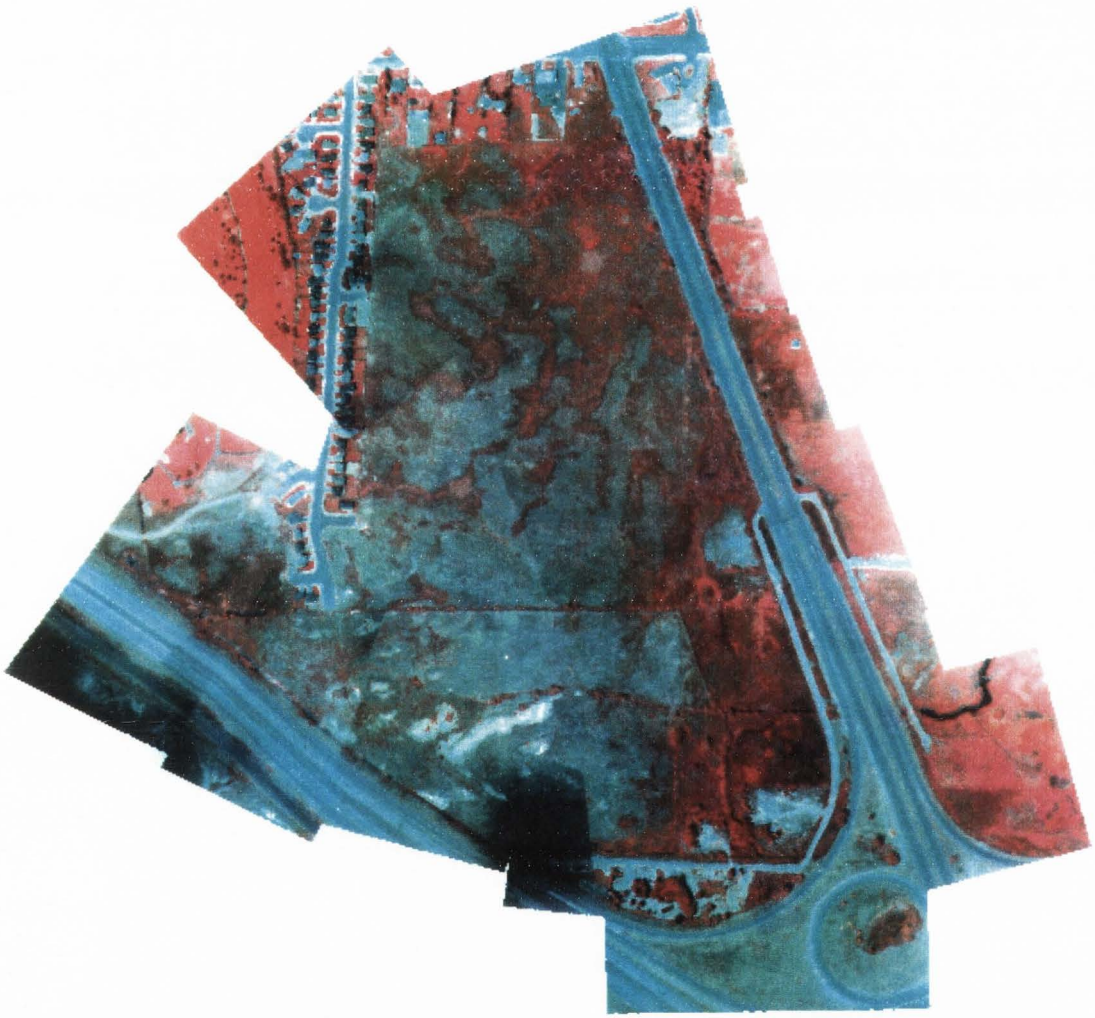

Figure 4. July 22, 1992 mosaic image.

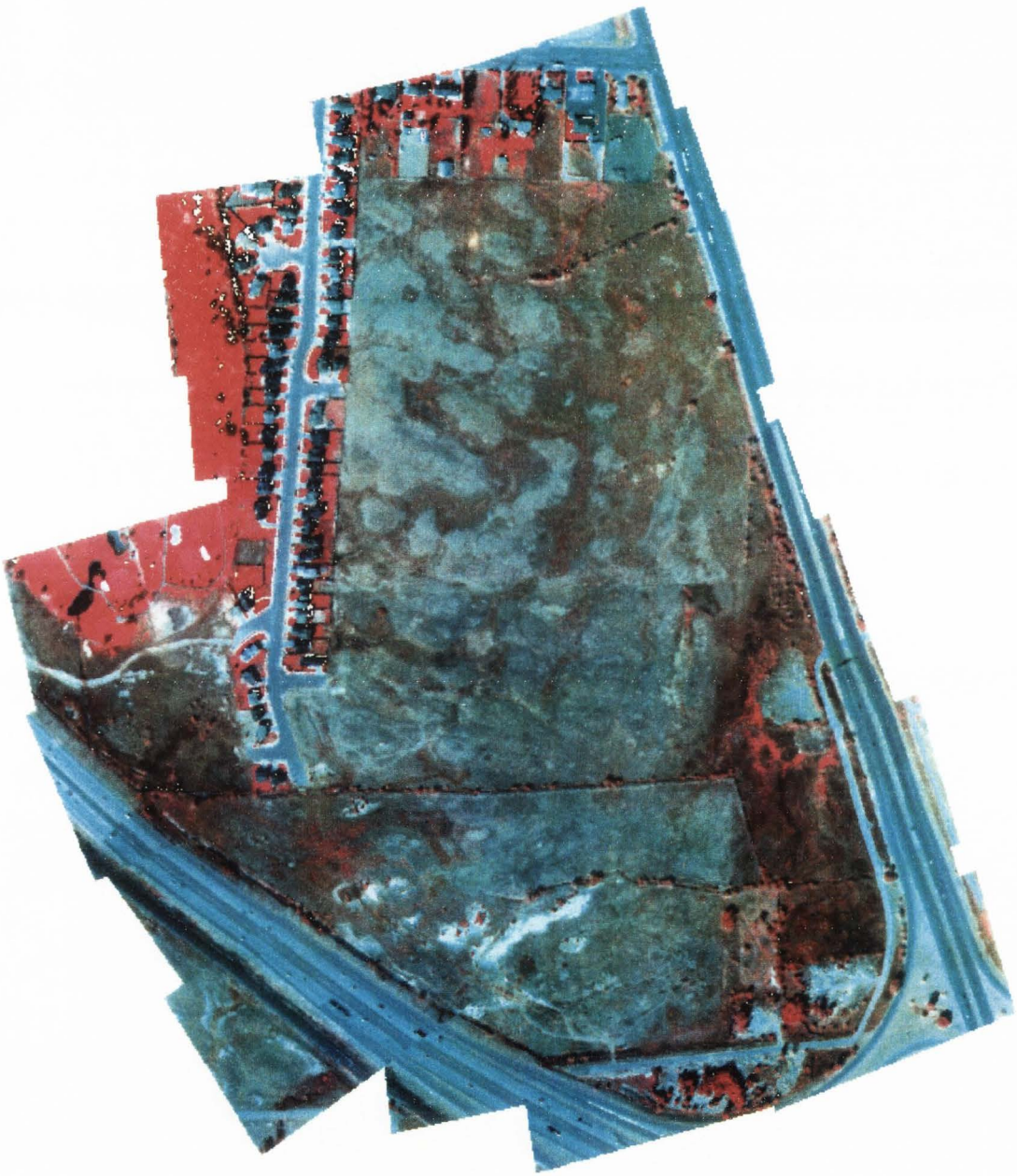

Figure 5. October 1, 1992 mosaic image.

Because the individual images were not radiometrically corrected, each 3-band composite was evaluated individually for the parametric methods. The resulting GIS image files were stitched to form mosaics for the three dates and rectified to a 1:24000 orthophoto[1] map for accuracy analysis. A fuzzy c-means program developed at Utah State University was modified to read the ERDAS file formats and the mosaic for each date was submitted to this method to produce a mosaiced GIS image for accuracy evaluation.

Parametric Techniques

Traditional classification of images has relied on parametric techniques (Foody, 1992). This project used three parametric techniques to cluster and classify the data. Individual 3-band composites were classified and the resulting classified images stitched together into a mosaic using the coordinate transformation matrices developed for forming the composite mosaics.

Supervised clustering

The first parametric technique was a supervised classification using operator-identified training sets and a Bayesian/maximum likelihood classifier. To determine the appropriate number of training sets, three 3-band composites were randomly selected from the first flight date. Spectral

---

[1]A map composed of geometrically corrected aerial photos.

signatures derived from the operator-selected, spectrally homogeneous, spatially contiguous pixel groups were tested for use as training sets. These test sets of spectral properties were evaluated with a transformed divergence separability index (equation [1]) (Swain and Davis, 1978) to determine if a sufficient number of classes were selected with no overlap.

$$D_{ij} = \frac{1}{2} tr\left((C_i - C_j)\left(C_i^{-1} - C_j^{-1}\right)\right) + \frac{1}{2} tr\left(\left(C_i^{-1} - C_j^{-1}\right)(\mu_i - \mu_j)(\mu_i - \mu_j)^T\right) \quad (1)$$

$$TD_{ij} = 2\left(1 - \exp\left(-\frac{D_{ij}}{8}\right)\right)$$

where i and j are the classes compared

C_i is the covariance matrix with values for bands t and u of signature i with n_i samples in the signature given by

$$\frac{1}{(n_i - 1)} \sum_{s=1}^{n_i} (x_{st} - \mu_{it})(x_{su} - \mu_{iu})^T$$

tr is the trace of the covariance matrix

μ_i is the mean for signature i

D_{ij} is the divergence

TD_{ij} is the transformed divergence.

Some test signature sets, for example signature 1 in test file 1 (see Figure 6), had saturated values in the IR band (brightness values of 255). These test signatures had a covariance matrix with zero values in one column and row, so the covariance matrix was not invertible for use in equation (1). These signatures were deleted from the test file prior to the transformed

divergence testing (see Appendixes A-C for transformed divergence values for evaluated signature pairs from the test files). By using the remaining test signatures with all band pair combinations, two-dimensional principal component plots of the clusters were viewed to evaluate test set signature overlap. Visual examination of these signature overlaps at two standard deviation units (see Figures 6-8) led to selection of a TD_{ij} threshold level of 1300. For example, in Figure 6, test signatures 9 and 13 have slight overlap in the band 1-3 and band 2-3 plots and significant overlap in the band 1-2 plot (band1 - near-IR, band2 - red, band3 - green), which corresponds to TD_{ij}=1775. In Figure 7, test signature 10 and 16 have significant overlap with a TD_{ij}=1228. Pairs of clusters with values lower than the 1300 threshold were considered inseparable and combined. This evaluation led to the selection of six to seven vegetational classes, two water classes, two shadow classes, three soil classes, and three to four man-made object classes to generate training sets for each 3-band composite.

The training sets were used in a Bayesian/maximum likelihood classifier (equation [2]) for clusters with multivariate normal distributions and the *a priori* probabilities set equal.

$$B_{ij} = \ln(p_j) - [0.5\ln(|C_j|)] - [0.5(x_i-\mu_j)^T(C_j^{-1})(x_i-\mu_j)] \quad (2)$$

where B_{ij} is the natural logarithm of the likelihood that sample *i* belongs to class *j*

p_j is the *a priori* probability that any element belongs to class *j*

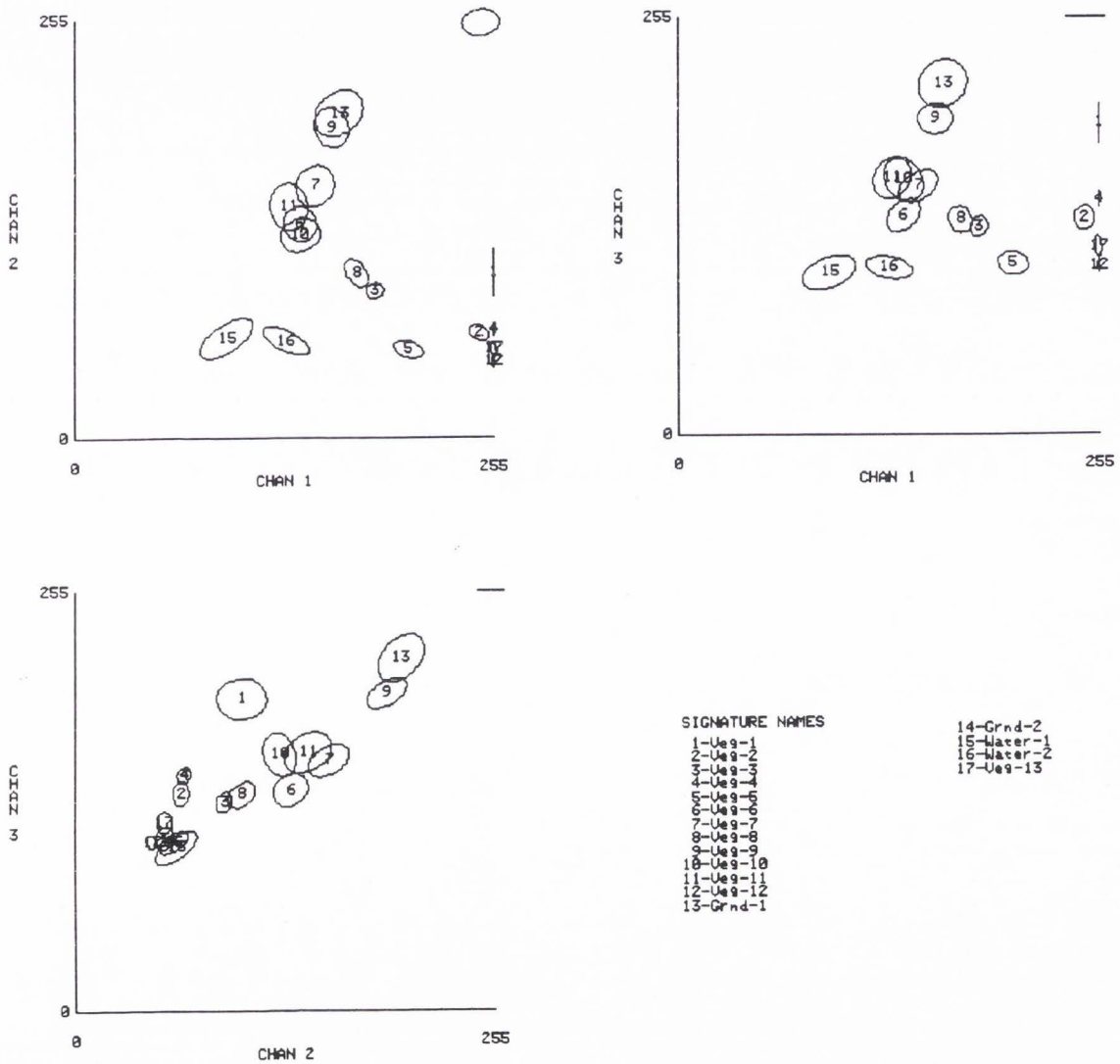

Figure 6. Cluster two-dimensional principal components for test file 1.

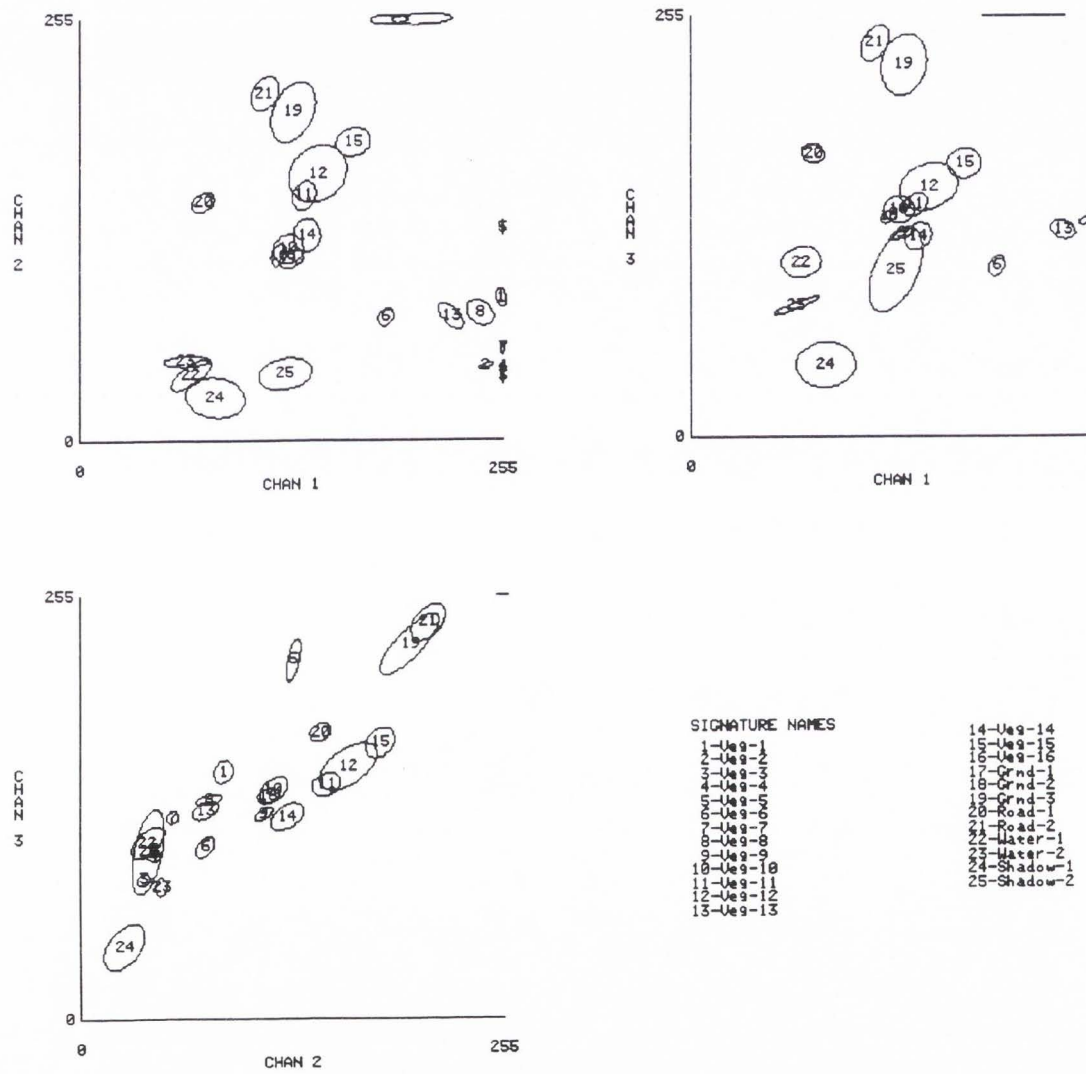

Figure 7. Cluster two-dimensional principal components for test file 2.

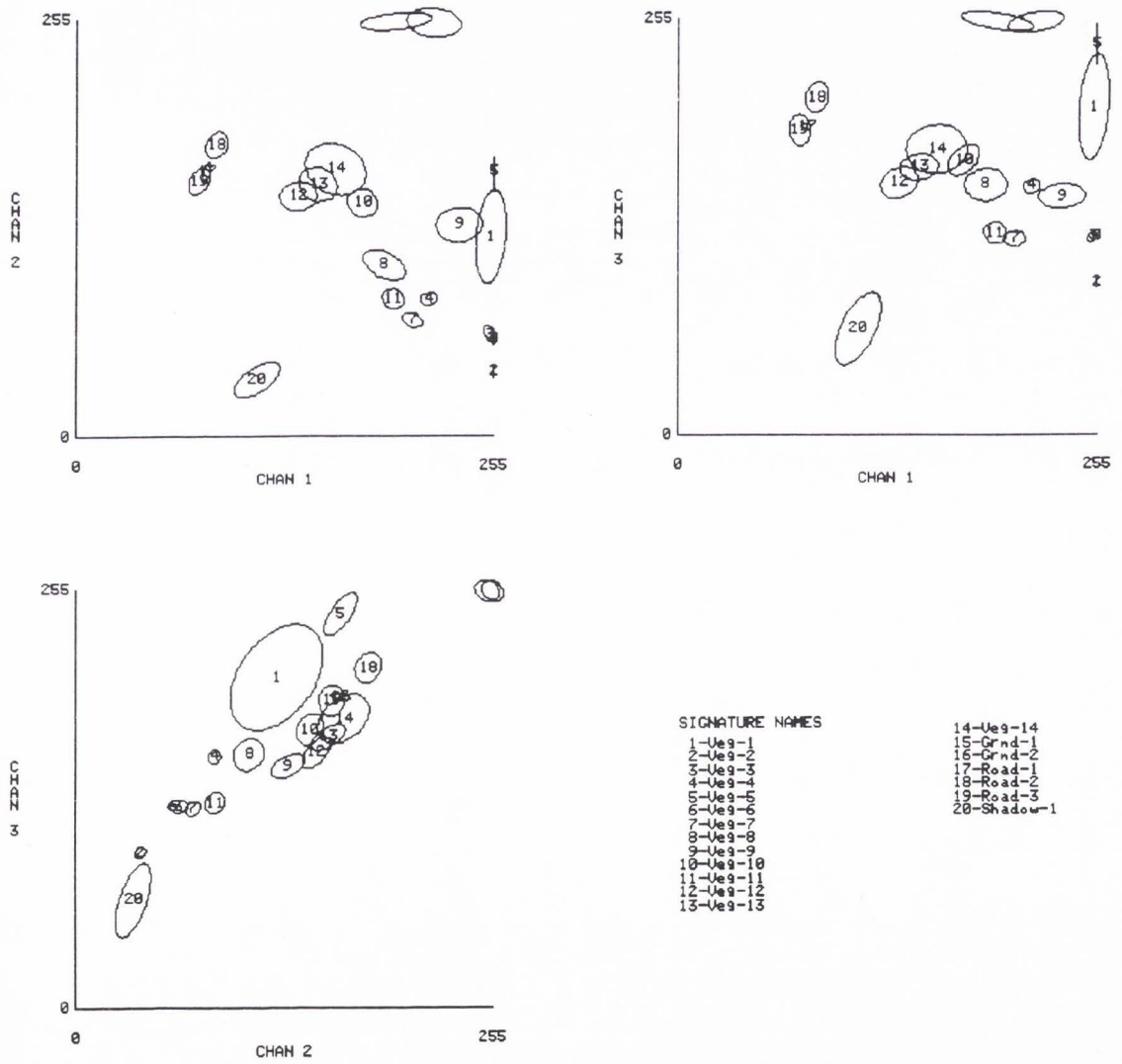

Figure 8. Cluster two-dimensional principal components for test file 3.

The sample *i* is placed in the class *j* for which B*ij* is a maximum. Histograms for selected signatures were examined to verify normality. In the three-dimensional spectral space, the training sets appear as ellipsoids of varying shape and size while the resulting decision boundaries to maximize B_{ij} are hyperquadrics (Duda and Hart, 1973).

ISODATA

The first of the unsupervised parametric methods involves the iterative solution of a Euclidian distance classifier with class membership recalculated based on the membership values assigned in the previous iteration (equation [3]). The first assignment of membership values to N

$$D_i = (x_i-\mu_j)^T(C_j)^{-1}(x_i-\mu_j)$$
$$u_j=\sum_{i=1}^{n} x_i/n \qquad (3)$$

user-defined clusters is accomplished by dividing the sample spectral space into N equal volumes oriented along the major principal component axis. The cluster membership values between successive iterations are compared for each sample. When the percentage of pixels whose classification does not change reaches a preassigned convergence threshold, the algorithm terminates. The ERDAS software also provides for the termination after a prespecified number of iterations to prevent hunting by the algorithm and a minimum number of samples for a valid cluster.

Based on the evaluation of required classes for the supervised method, the number of classes for ISODATA was set at 20. Setting the convergence threshold at 95% and maximum number of iterations at 24 yielded a minimum of 92% convergence for all files. Following clustering of the images with ISODATA, the training sets were evaluated using transformed divergence (equation [1]). Again, a threshold of 1300 was used to evaluate signature pairs. In cases where two of the possible pair comparisons among three clusters fell below 1300 and the remaining pair comparison fell below 1400, the clusters were judged to be indistinguishable and combined. If $TD_{ij} > 1400$ for the remaining pair, then the signature which was common between the two pair comparisons with $TD_{ij} < 1300$ was judged to overlap the other two clusters and deleted. This gave a range of 10 to 19 (typically 14) clusters for each 3-band composite. The clusters from this evaluation/combination were used as the training sets in a Euclidian distance classifier. A Euclidian classifier was chosen because of its similarity to the ISODATA clustering routine.

Statistical clustering

This algorithm steps nonoverlapping 3-by-3 windows across the image and performs a spatial homogeneity test to determine a user-specified number of signatures, N. The standard deviation, s_i, of each band for each window is compared against a lower bound. This lower band prevents ill-conditioned covariance matrices in the classification routines that are used

with the signatures generated (covariance matrices for the classification algorithms are calculated as described above for the transformed divergence). If this test is passed, s_i is tested against an upper bound, G, to determine its use in fixing the clusters (equation [4]).

$$G = maximum \ (U, \ m_i \cdot V/100) \qquad (4)$$

where U is a user-defined value to ensure windows with low means are not discounted as homogeneous

m_i is the mean for band *i* in the window

V is the user-selectable coefficient of variation (percentage) used with the mean as an alternative upper limit

If s_i<G, the window is considered homogeneous in band *i*, and if all bands are homogeneous, the window is used in cluster determination. Each window is initially considered a separate cluster until N+1 clusters are found. Windows are pair-wise compared and those whose scaled spectral distance, S_x, (equation [5]) exceeds a user-specified maximum are merged (ERDAS, 1991).

$$S_x = \sqrt{\sum \frac{(\mu_{ai} - \mu_{bi}) \ (W_{ai} + W_{bi})^2}{0.05 \ (W_{ai}\mu_{ai} + W_{bi}\mu_{bi})}} \qquad (5)$$

where W_{ai},W_{bi} are the number of windows in cluster a,b band i

μ_{ai},μ_{bi} are the means of cluster a,b band i

To allow comparison with the unsupervised ISODATA, the user-defined upper limit for number of classes was set to 20. The resulting clusters were submitted to transformed divergence testing as described above for ISODATA, and again yielded 10 to 20 classes (typically 14) for each 3-band composite. The resulting training sets were then used for image classification with a Bayesian/maximum likelihood classification decision rule (Duda and Hart, 1973; ERDAS, 1991).

Fuzzy c-Means Clustering

Classical clustering techniques requires that each pixel be a member of only one class. Class membership value, u_{ik}, for an element, x_k, is assigned a value of 0 or 1 to denote its membership in a class, c (equation [6]).

$$u_{ik} = \begin{cases} 1 \text{ if sample } k \text{ belongs to class } c \\ 0 \text{ if sample } k \text{ does not belong to class } c \end{cases} \quad (6)$$

with the conditions

$$\sum_{i=1}^{c} u_{ik} = 1 \quad \text{for every sample } k$$
$$\sum_{k=1}^{n} u_{ik} > 0 \quad \text{for every cluster } i \quad (7)$$

The first condition ensures that the sample belongs to at least one and only one cluster and the second condition requires that all clusters must have at least one member.

In nature, divisions are not so neat and pixels generally contain properties of more than one of the classes of interest. A new approach which overcomes this shortcoming is the use of fuzzy sets logic. Fuzzy logic allows a pixel to take on values from more than one cluster. In fuzzy set clustering the membership value, u_{ik}, can take on any value between 0 and 1 (equation [8]) with the conditions listed in equation (7). The first

$$u_{ik} \in \{0,1\} \quad for \quad every \quad i \; and \; k \qquad (8)$$

condition limits each sample to one total class while the second condition ensures that the class is not an empty set. If the data set is represented by n d-dimensional vectors, x_k, then the membership values, u_{ik}, can be calculated by equation (9) where D_{ik} represents the measure of the distance between the sample and the cluster center (Gunderson and Jacobsen, 1983).

$$u_{ik} = 1/\sum_{j=1}^{c}\left(\frac{D_{ik}}{D_{ij}}\right)^{\frac{2}{m-1}} \quad (D_{ij}\neq 0,\ m>1) \qquad (9)$$

For this application the distance vector is defined as:

$$D_{ik} = \left(|x_k - \mu_i|^2\right)^{1/2} \qquad (10)$$

with cluster centers

$$\mu_i = \sum_{k=1}^{n} (u_{ik})^m x_k \Big/ \sum_{k=1}^{n} (u_{ik})^m \qquad (11)$$

Equations (10) and (11) describe the Euclidian distance to the center of the fuzzy clusters. More generalized forms of equation (10) can be used to specify differing distance measurements as well as cluster shapes (Bezdek et al., 1981). The exponential weight factor, m, determines how "fuzzy" each cluster is. As m approaches 1, the algorithms act as a classical Boolean classifier. As the value of m increases, samples that are only marginally in the cluster have less influence in defining the cluster centers (Gunderson, 1983). The u_{ik} values are analogous to the covariance matrix in a conventional parametric method. The use of a Euclidian distance measure with its squared term and the analogy to covariance suggest a "natural" value of 2 for m (Gunderson, 1994). For this application, a value of 2 was selected for use in the fuzzy c-means clustering algorithm.

Fuzzy set logic is relatively untested in the world of remotely sensed image classification. The only work known in this field was performed in England where Foody (1992) used a supervised fuzzy c-means algorithm (m=1.25) and a Mahalanobis norm to classify lowland heaths. Although his results were promising, with 100% accuracies, the use of the same sample set for training and accuracy testing makes the accuracy estimate questionable.

This investigation used a modified maximum membership clustering protocol. Each class was examined to determine which of the fuzzy classes could be combined or considered indistinct. These class memberships for these classes were combined and a classified file produced where each pixel was assigned to the class with the highest membership value.

Accuracy Assessment

Results for the two accuracy testing methods are given in terms of contingency tables and omission/commission tables (error matrices) (see Results section). The results from all dates for each technique produced 24 contingency tables. In order to reduce the amount of analyzable data to a more easily seen form, the kappa, κ, coefficient was used to reduce the data in each contingency table to a single value. The κ measures how much better the classification algorithm is than a random assignment of features to classes with the same class-to-class ratios as the tested classification. For example, if the true image had a 1:1 ratio for features A and B, a random assignment of features would be expected to assign 50% of the A objects and 50% of the objects to the correct classes. This would give an overall classification accuracy of 50% with 50% of both class A and B misclassified. A classification decision rule which correctly assigned 75% of objects A and B (improperly assigning 25% of each of the true classes) of the

same set would correctly assign 50% of the objects missed by the random classifier. This would equate to a kappa of (0.75-0.50)/(1.0-0.50)=0.50.

Kappa values, κ, were calculated using equations (12) and (13) as proposed by Cohen (1960) (for other methods to calculate kappa, see Foody [1992]).

$$\kappa = \frac{\theta_1 - \theta_2}{1 - \theta_2} \tag{12}$$

$$\begin{aligned} \theta_1 &= \sum_{i=1}^{N} x_{ii} / \sum_{i,j=1}^{N} x_{ij} \\ \theta_2 &= [\sum_{i=1}^{N} (\sum_{j=1}^{N} x_{ij}) (\sum_{j=1}^{N} x_{ji})] / (\sum_{i,j=1}^{N} x_{ij})^2 \end{aligned} \tag{13}$$

where θ_1 is the overall accuracy of the classification

θ_2 is the accuracy of a random classifier with the same marginal values (class-to-class ratios) as the tested classifier

x_{ij} is the number of samples in position i,j of the contingency table

Values for the κ large sample variance (σ_κ^2 in Tables 7 and 8) were calculated using equation (14) (Bishop, Fienberg, and Holland, 1975).

$$\sigma_\kappa^2 = \frac{1}{N}\{\frac{\theta_1(1-\theta_1)}{(1-\theta_2)^2} + \frac{2(1-\theta_1)(2\theta_1\theta_2-\theta_3)}{(1-\theta_2)^3} + \frac{(1-\theta_1)^2(\theta_4-4\theta_2^2)}{(1-\theta_2)^4}\} \tag{14}$$

where N is the number of values x_{ij} in the contingency table

and

$$\theta_3 = \sum_{i=1}^{N} \frac{x_{ii}}{N} \left(\sum_{j=1}^{N} \frac{x_{ij}}{N} + \sum_{j=1}^{N} \frac{x_{ji}}{N} \right)$$

$$\theta_4 = \sum_{i,j=1}^{N} \frac{x_{ij}}{N} \left(\sum_{k=1}^{N} \frac{x_{jk}}{N} + \sum_{k=1}^{N} \frac{x_{ki}}{N} \right)^2 \qquad (15)$$

Comparison of multiple κ values was performed using methods outlined by Fleiss (1981). First, a common kappa is estimated from g values using equation (16).

$$\overline{\kappa} = \sum_{m=1}^{g} \frac{\kappa_m}{\sigma_{\kappa_m}^2} \Big/ \sum_{m=1}^{g} \frac{1}{\sigma_{\kappa_m}^2} \qquad (16)$$

Next, the null hypothesis of equal κ's is tested using the chi-square distribution at the α level of significance with g-1 degrees of freedom as calculated by equation (17).

$$\chi^2_{\alpha, g-1} = \sum_{m=1}^{g} \frac{(\kappa_m - \overline{\kappa})}{\sigma_{\kappa_m}^2} \qquad (17)$$

RESULTS

Classification Accuracy

Data from the ground-based sample points used in original jurisdictional delineation were used in the recoding and in the ground point comparison accuracy test described below. These sample points were selected by the wetland consulting firm that produced the original jurisdictional delineation and can be seen in Figure 9 (Grah and Crane, 1991). The data for the sample points included soil type, hydrologic characterization, and vegetational type listed by percentage areal coverage. Jurisdictional delineation requirements mandate the presence of hydric soils, wetland hydrological conditions, and hydric vegetation. The wavelengths used by the mutltispectral videography system do not penetrate the surface. Thus determination of subsurface conditions is not possible and direct information concerning soil characteristics and subsurface hydrology is unavailable. As a result, only the vegetation information for each of the original sample points was used for evaluation.

Areal vegetational coverage for the sample points was used to divide the points into wetland and upland categories. Based only on this vegetation criterion (ignoring the soil and hydrology requirements), five of the upland points were moved to the wetland category. These five sample points actually had predominantly wetland vegetation, but lacked the

supporting soils and/or hydrology that resulted in their classification as upland in the original jurisdictional delineation. By using the vegetation-only criterion, these five points were recoded as wetland for the recoding and accuracy comparison. As shown in Figure 9, these ground sample points were randomly divided into a training set (yellow points) and a verification set (white points).

The training set was used in recoding of classified files into six thematic groups identified. From ground site visits and the visual inspection of the imagery, six thematic classes were initially selected for use in analysis: (1) wetland vegetation, (2) open water, (3) upland vegetation, (4) open ground, (5) man-made objects, and (6) shadow. Classes produced in each of the individual images for the parametric methods and the mosaic for the fuzzy c-means were evaluated against the training set and placed into one of these six thematic classes. The ground truth map from the jurisdictional delineation contained only upland and wetland information, so for the final accuracy assessment, these six thematic classes were evaluated as wetland and upland or ignored as background. Shallow areas of open water are denoted as wetlands in the Corps permitting process, so the open water class was compared as wetland. Areas exhibiting open ground properties were compared as upland since they did not meet vegetation requirements. Man-made objects and deep shadows were ignored as background. Figures 10-12 show the final recoded and registered

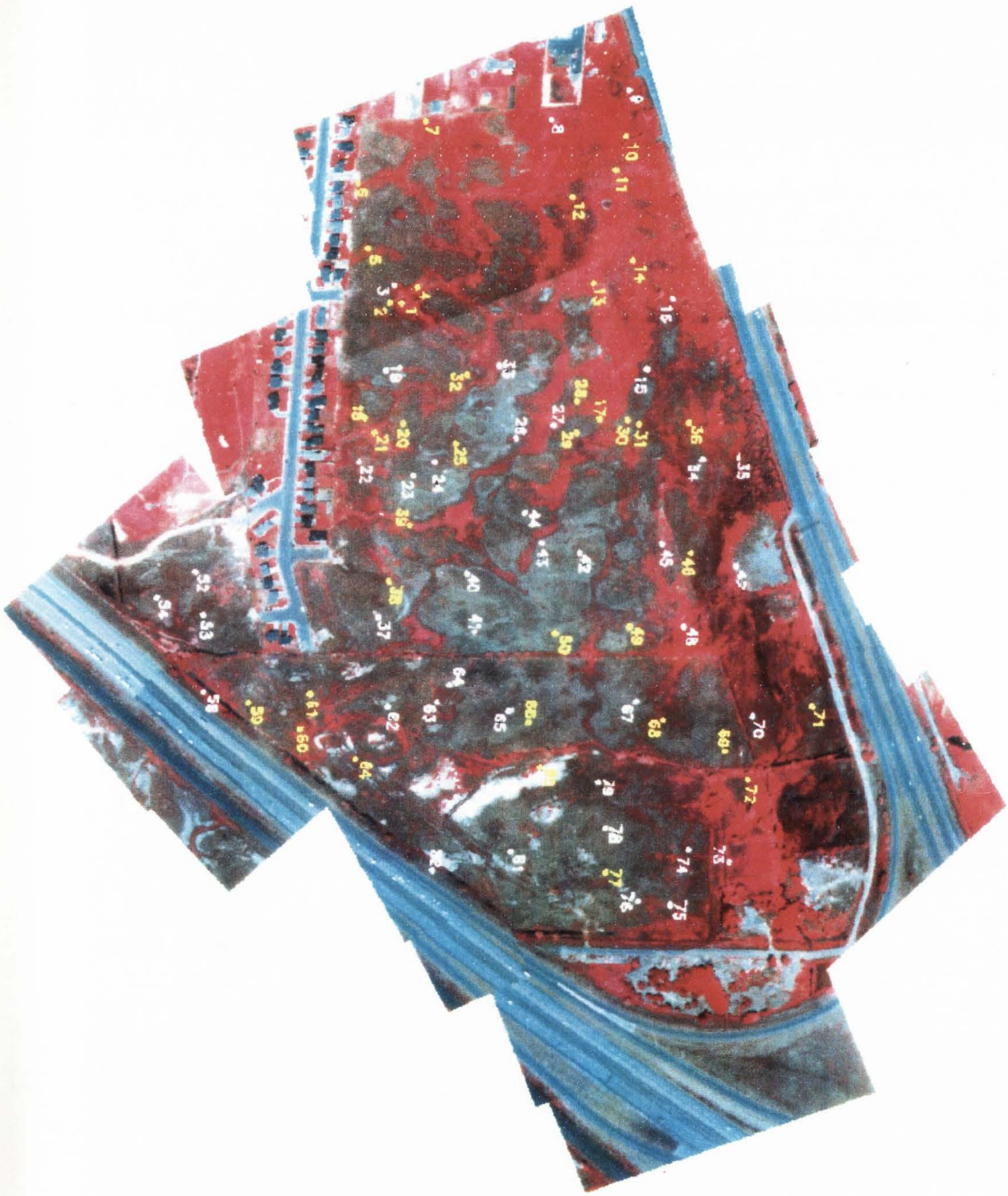

Figure 9. Location of ground-based sample points divided into training set (yellow points) and verification set (white points).

Figure 10. June 2, 1992 classified imagery. (key: wetland - red, upland - green, background - black)

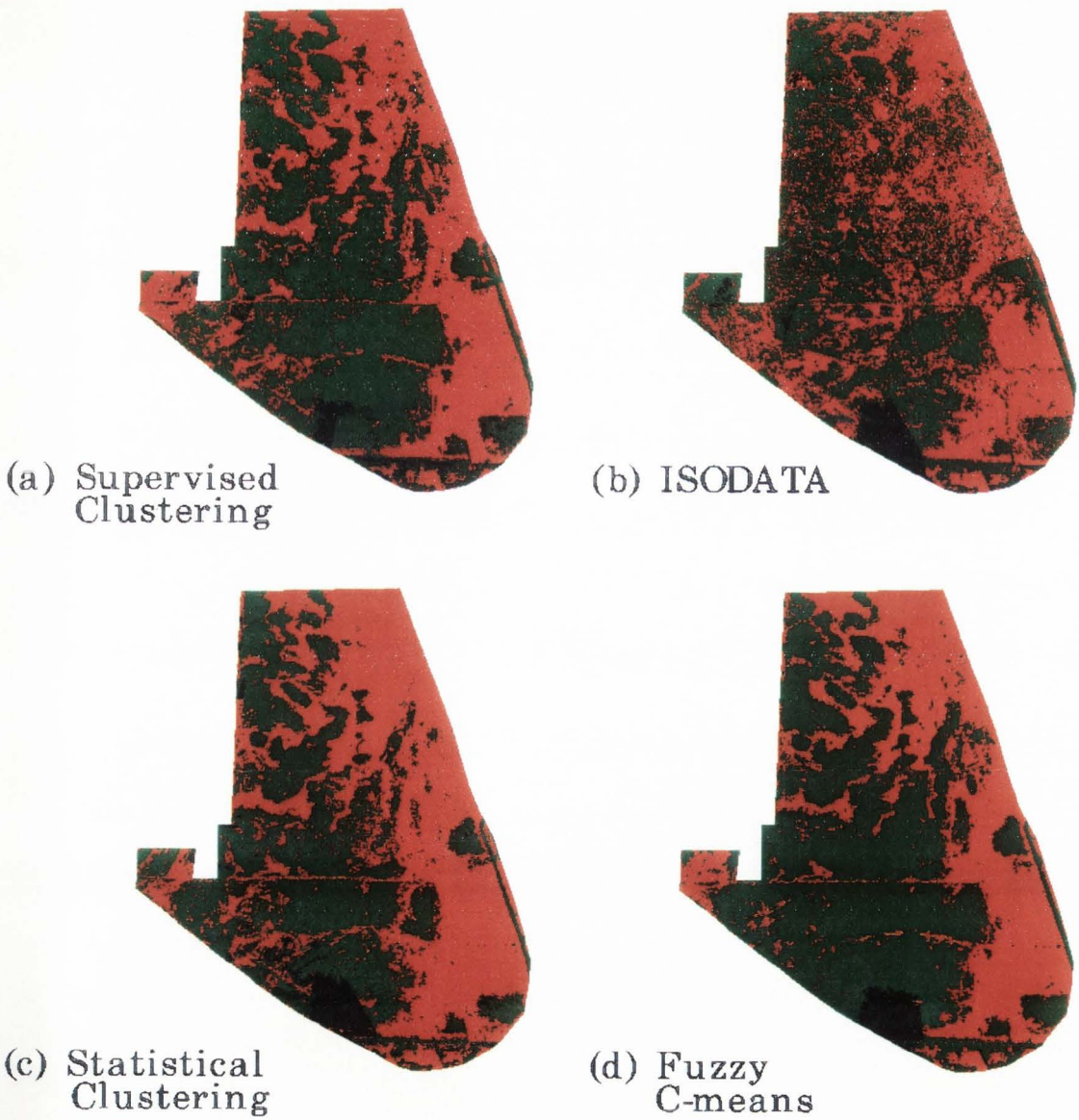

Figure 11. July 22, 1992 classified imagery. (key: wetland - red, upland - green, background - black)

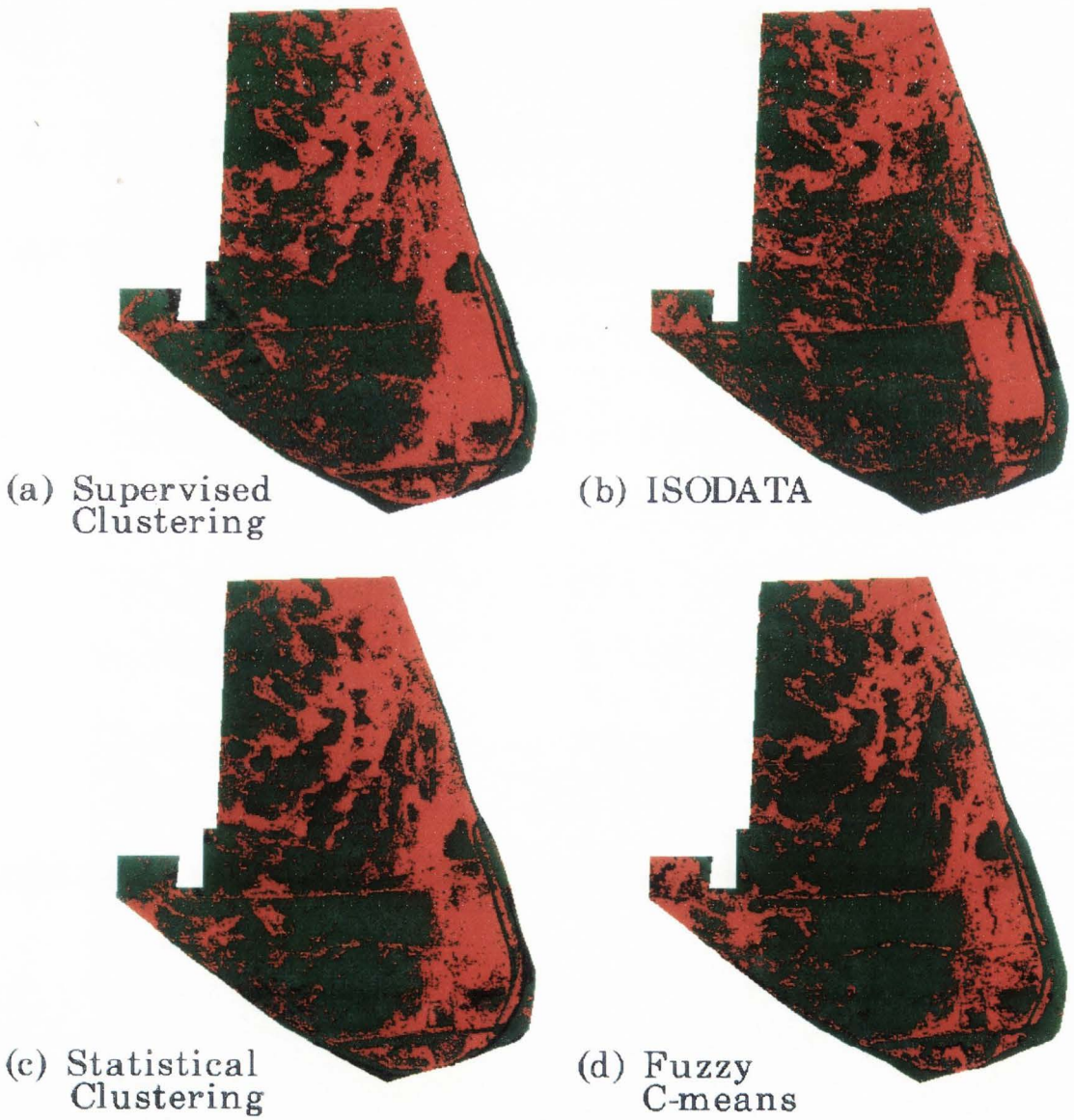

Figure 12. October 1, 1992 classified imagery. (key: wetland - red, upland - green, background - black)

mosaics. These recoded mosaics were submitted to the two testing methods, ground point comparison and random window comparison, described below.

Ground Point Comparison

The first method involved comparing the mosaiced and registered images to the verification set of 38 points described above. The ground-based sample points were displayed on a set of the classified imagery in hard copy format. Five individuals were asked to use the verification set to determine accuracies for each classification technique for each date. The individuals included one U.S. Forest Service biologist and four individuals familiar with multispectral imagery as used with natural systems evaluation. The individuals evaluated the verification points as either upland or wetland on the classified mosaiced images. The point's selected class from each evaluator was tabulated against the correct class (ground truth) from the original classification. The average of these responses was compiled in 2-by-2 contingency tables (see Tables 1-3). For example, in Table 1a, 18.8 wetland points were correctly identified as such for the possible 25 wetland points in the verification set. Upland points were correctly identifies as upland for 9.4 of the 13 points. In addition to the contingency tables, an error matrix was calculated for each contingency table and is presented immediately following its contingency table. The omission error is the percentage of actual wetland points (ground truth)

Table 1. June 2 flight – ground point comparison

a. Supervised clustering, Bayesian classifier

Contingency Table		Image	
		Wetland	Upland
Ground Truth	Wetland	18.8	6.2
	Upland	3.6	9.4

Error Matrix	Omission Errors	Commission Errors	Correct
Wetland	24.8%	14.4%	75.2%
Upland	27.7%	47.7%	72.3%
Overall	25.8%	25.8%	74.2%

b. ISODATA clustering, Euclidean classifier

Contingency Table		Image	
		Wetland	Upland
Ground Truth	Wetland	17.0	8.0
	Upland	3.8	9.2

Error Matrix	Omission Errors	Commission Errors	Correct
Wetland	32.0%	15.2%	68.0%
Upland	29.2%	61.5%	70.8%
Overall	31.1%	31.1%	68.9%

Table 1. (cont'd)

c. Statistical clustering, Bayesian classifier

Contingency Table		Image	
		Wetland	Upland
Ground Truth	Wetland	17.8	7.2
	Upland	4.6	8.4

Error Matrix	Omission Errors	Commission Errors	Correct
Wetland	28.8%	18.4%	71.2%
Upland	35.4%	55.4%	64.6%
Overall	31.1%	31.1%	68.9%

d. Fuzzy c-means clustering and maximum membership classifier

Contingency Table		Image	
		Wetland	Upland
Ground Truth	Wetland	17.6	7.4
	Upland	3.4	9.6

Error Matrix	Omission Errors	Commission Errors	Correct
Wetland	29.6%	13.6%	70.4%
Upland	26.2%	56.9%	73.8%
Overall	28.4%	28.4%	71.6%

Table 2. July 22 flight – ground point comparison

a. Supervised clustering, Bayesian classifier

Contingency Table		Image	
		Wetland	Upland
Ground Truth	Wetland	14.2	10.8
	Upland	3.2	9.8

Error Matrix	Omission Errors	Commission Errors	Correct
Wetland	43.2%	12.8%	56.8%
Upland	24.6%	83.1%	75.4%
Overall	36.8%	36.8%	63.2%

b. ISODATA clustering, Euclidean classifier

Contingency Table		Image	
		Wetland	Upland
Ground Truth	Wetland	14.8	10.2
	Upland	5	8

Error Matrix	Omission Errors	Commission Errors	Correct
Wetland	40.8%	20.0%	59.2%
Upland	38.5%	78.5%	61.5%
Overall	40.0%	40.0%	60.0%

Table 2. (cont'd)

c. Statistical clustering, Bayesian classifier

Contingency Table		Image	
		Wetland	Upland
Ground Truth	Wetland	17.2	7.8
	Upland	4.4	8.6

Error Matrix	Omission Errors	Commission Errors	Correct
Wetland	31.2%	17.6%	68.8%
Upland	33.8%	60.0%	66.2%
Overall	32.1%	32.1%	67.9%

d. Fuzzy c-means clustering and maximum membership classifier

Contingency Table		Image	
		Wetland	Upland
Ground Truth	Wetland	15.8	9.2
	Upland	4.2	8.8

Error Matrix	Omission Errors	Commission Errors	Correct
Wetland	36.8%	16.8%	63.2%
Upland	32.3%	70.8%	67.7%
Overall	35.3%	35.3%	64.7%

Table 3. October 1 flight – ground point comparison

a. Supervised clustering, Bayesian classifier

Contingency Table		Image	
		Wetland	Upland
Ground Truth	Wetland	15.8	9.2
	Upland	4.8	8.2

Error Matrix	Omission Errors	Commission Errors	Correct
Wetland	36.8%	19.2%	63.2%
Upland	36.9%	70.8%	63.1%
Overall	36.8%	36.8%	63.2%

b. ISODATA clustering, Euclidean classifier

Contingency Table		Image	
		Wetland	Upland
Ground Truth	Wetland	11.2	13.8
	Upland	5.4	7.6

Error Matrix	Omission Errors	Commission Errors	Correct
Wetland	55.2%	21.6%	44.8%
Upland	41.5%	106.2%	58.5%
Overall	50.5%	50.5%	49.5%

Table 3. (cont'd)

c. Statistical clustering, Bayesian classifier

Contingency Table		Image	
		Wetland	Upland
Ground Truth	Wetland	13.8	11.2
	Upland	3.6	9.4

Error Matrix	Omission Errors	Commission Errors	Correct
Wetland	44.8%	14.4%	55.2%
Upland	27.7%	86.2%	72.3%
Overall	38.9%	38.9%	61.1%

d. Fuzzy c-means clustering and maximum membership classifier

Contingency Table		Image	
		Wetland	Upland
Ground Truth	Wetland	14.6	10.4
	Upland	2.2	10.8

Error Matrix	Omission Errors	Commission Errors	Correct
Wetland	41.6%	8.8%	58.4%
Upland	16.9%	80.0%	81.5%
Overall	33.2%	33.2%	66.8%

that are misidentified as upland (6.2/25=24.8%). The commission error is the number of points identified as wetland that are in fact upland as a percentage of the actual number of wetland points (3.6/25=14.4%). The values in the correct column are the percentage of wetland points from the verification set that were correctly identified (18.8/25=75.2%).

Random Window Comparison

The second method used to determine the accuracy of the classification was to compare pixels on the classified image to corresponding points on the registered ground truth map (Figure 13). The following discussion is for a generic registered mosaic with all 12 of the registered mosaics (Figures 10-12) submitted to the same process. In order not to lose or modify the brightness values for each pixel due to resampling if the spectral imagery were scaled to a map base, a digitized copy of the ground truth map was rescaled (using nearest neighbor resampling) to match the resolution of each registered mosaic (0.69 m for June, 0.81 m for July, and 0.56 m for October). Because the resultant resolution exceeded the national mapping standards, a 5-by-5 pixel window (3.45 m x 3.45 m for June, 4.05 m x 4.05 m for July, and 2.30 m x 2.30 m for October) was used to more closely represent the map resolution.

The 5-by-5 window was randomly placed on the same location on both the ground truth map and the registered mosaic to compare classes. The

Figure 13. Ground truth map from original jurisdictional delineation (Grah and Crane, 1991).

software written for this comparison allowed a purity threshold for the window to be specified. This threshold set the minimum percentage for which a class must dominate the window in the truth and image files in order for the classes within the two windows to be compared. The test was performed in 5% increments from 0% to 100% for each date and classification method combination. For each test, 5000 windows were selected with random replacement. The responses for each date and classification method were tabulated in contingency tables and error matrices as described for the ground point comparison. Again to reduce the amount of data, a κ value was calculated for each contingency table. These κ's were graphed against the purity threshold and are presented in Figures 14-16. As the threshold decreases, the κ value drops rapidly toward an asymptotic value at about 50-60%. Because the definition for vegetation predominance in a jurisdictional wetlands requires $\geq$51% areal coverage for wetland vegetation, the classified mosaics were compared with a 51% threshold. The contingency table and error matrices are presented in Tables 4-6. Due to the asymptotic response of the κ as the purity threshold drops, accuracy values predicted with the random window comparison are believed to be conservative.

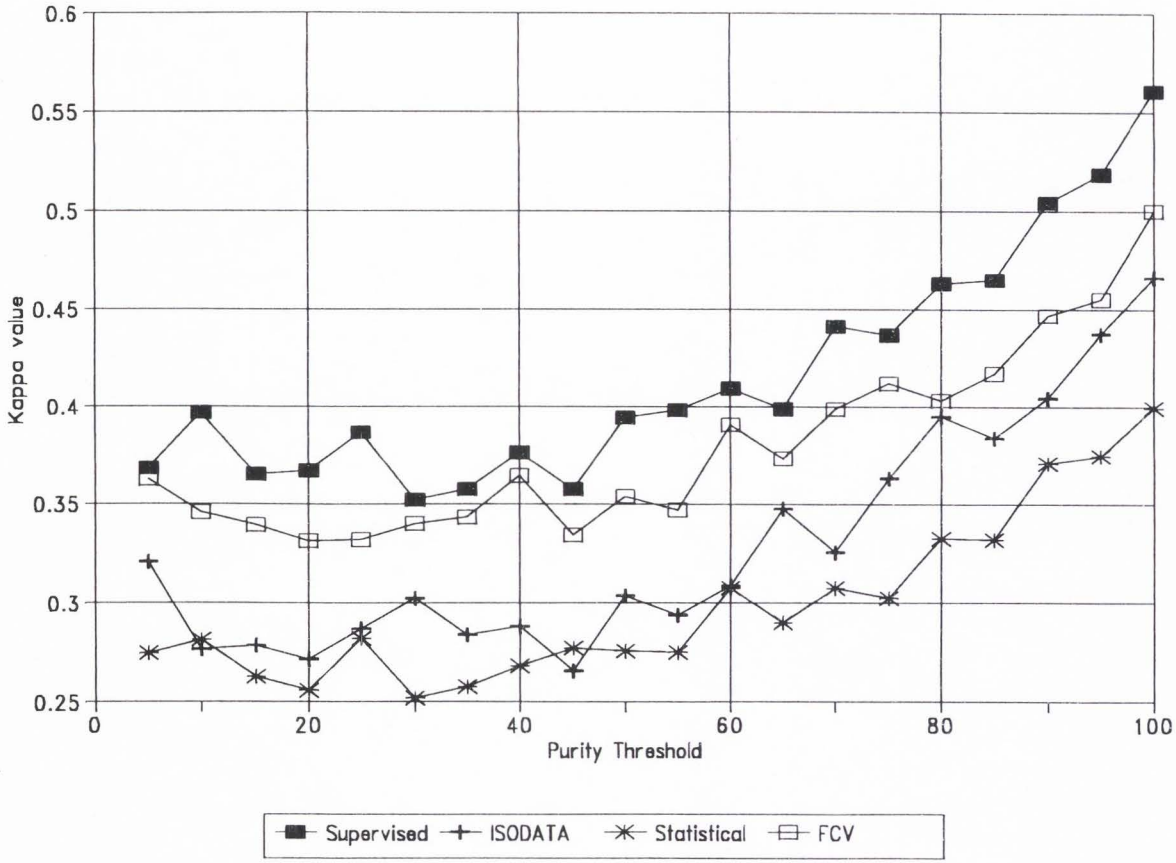

Figure 14. June 2 flight – kappa values vs purity threshold for 5-by-5 random window comparison.

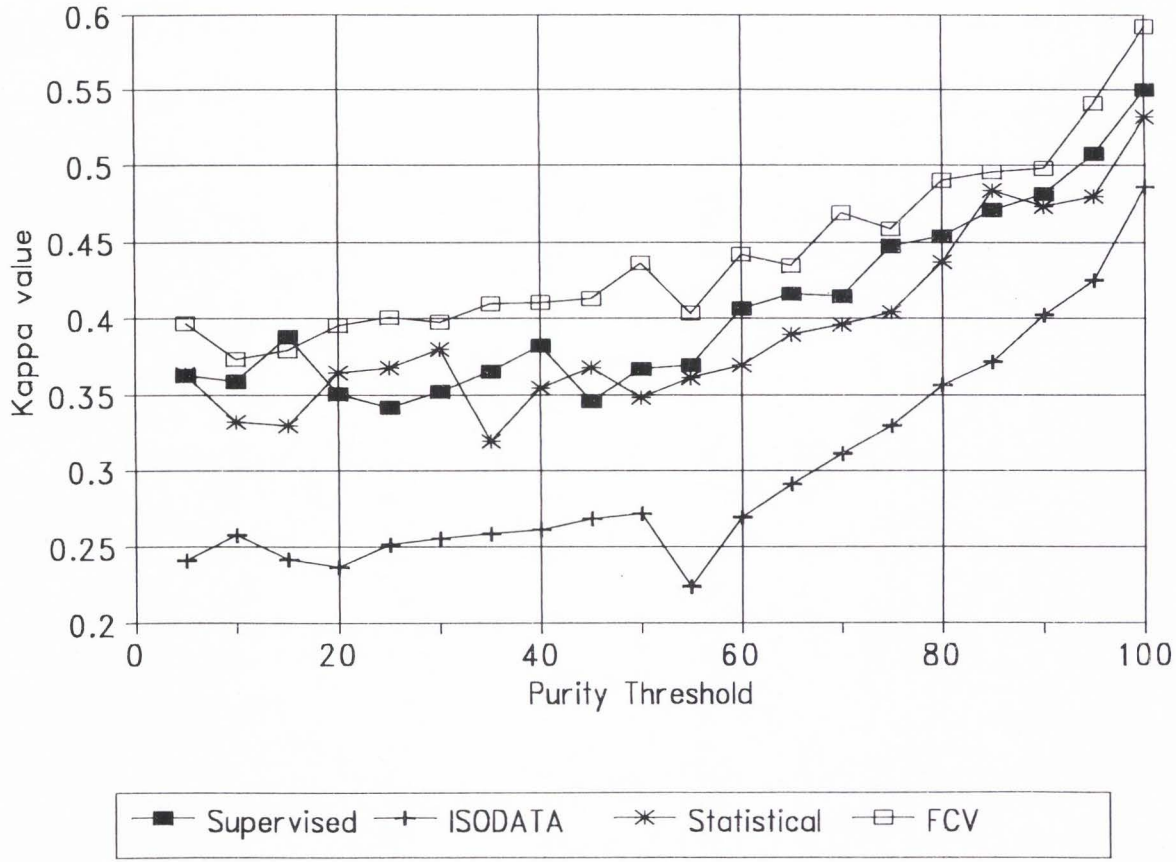

Figure 15. July 22 flight – kappa values vs purity threshold for 5-by-5 random window comparison.

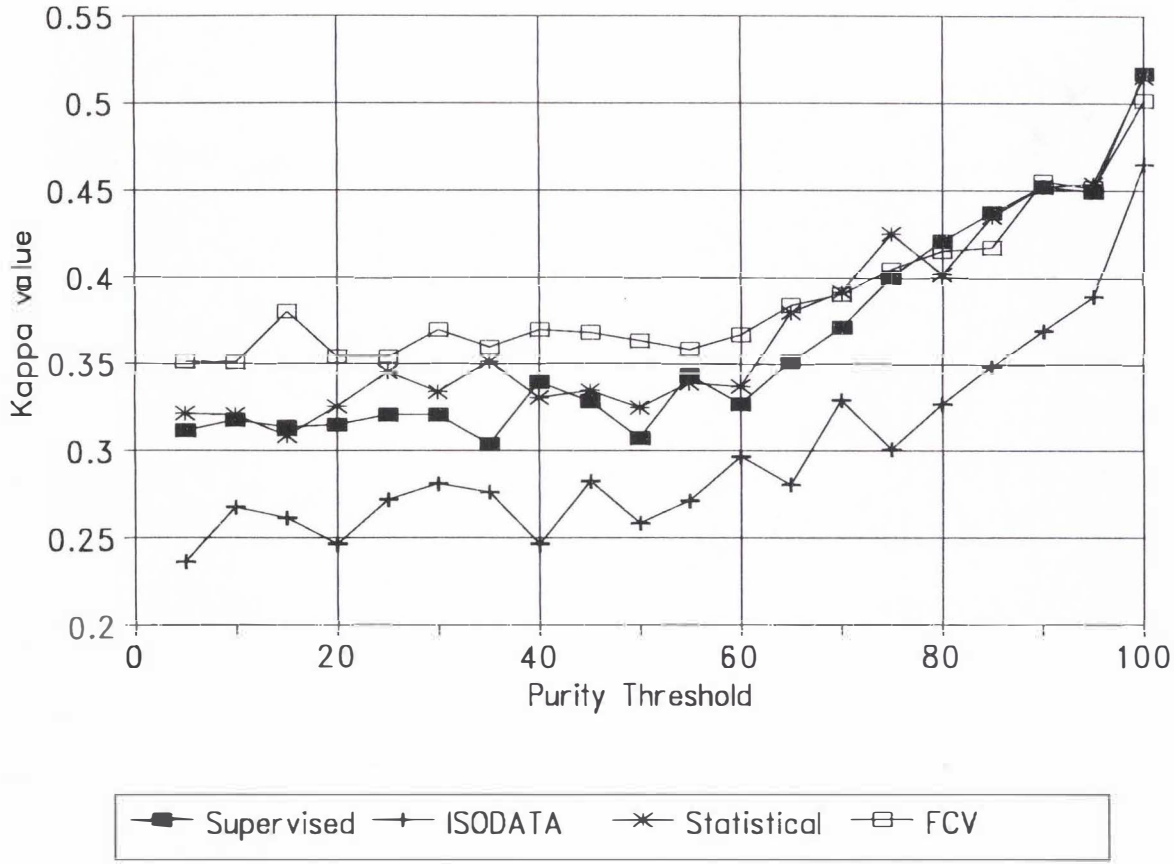

Figure 16. October 1 flight – kappa values vs purity threshold for 5-by-5 random window comparison.

Table 4. June 2 flight – random window comparison

a. Supervised clustering, Bayesian classifier

Contingency Table		Image	
		Wetland	Upland
Ground Truth	Wetland	1764	753
	Upland	826	1657

Error Matrix	Omission Errors	Commission Errors	Correct
Wetland	29.9%	31.9%	70.1%
Upland	33.3%	31.2%	66.7%
Overall	31.6%	31.6%	68.4%

b. ISODATA clustering, Euclidean classifier

Contingency Table		Image	
		Wetland	Upland
Ground Truth	Wetland	1710	804
	Upland	988	1498

Error Matrix	Omission Errors	Commission Errors	Correct
Wetland	32.0%	36.6%	68.0%
Upland	39.7%	34.9%	60.3%
Overall	35.8%	35.8%	64.2%

Table 4. (cont'd)

c. Statistical clustering, Bayesian classifier

Contingency Table		Image	
		Wetland	Upland
Ground Truth	Wetland	1820	690
	Upland	1072	1418

Error Matrix	Omission Errors	Commission Errors	Correct
Wetland	27.5%	37.1%	72.5%
Upland	43.1%	32.7%	56.9%
Overall	35.2%	35.2%	64.8%

d. Fuzzy c-means clustering and maximum membership classifier

Contingency Table		Image	
		Wetland	Upland
Ground Truth	Wetland	1686	801
	Upland	830	1683

Error Matrix	Omission Errors	Commission Errors	Correct
Wetland	32.2%	33.0%	67.8%
Upland	33.0%	32.3%	67.0%
Overall	32.6%	32.6%	67.4%

Table 5. July 22 flight – random window comparison

a. Supervised clustering, Bayesian classifier

Contingency Table		Image	
		Wetland	Upland
Ground Truth	Wetland	1601	901
	Upland	660	1838

Error Matrix	Omission Errors	Commission Errors	Correct
Wetland	36.0%	29.2%	64.0%
Upland	26.4%	32.9%	74.6%
Overall	31.2%	31.2%	68.8%

b. ISODATA clustering, Euclidean classifier

Contingency Table		Image	
		Wetland	Upland
Ground Truth	Wetland	1609	910
	Upland	973	1508

Error Matrix	Omission Errors	Commission Errors	Correct
Wetland	36.1%	37.7%	63.9%
Upland	39.2%	37.6%	60.8%
Overall	37.7%	37.7%	62.3%

Table 5. (cont'd)

c. Statistical clustering, Bayesian classifier

Contingency Table		Image	
		Wetland	Upland
Ground Truth	Wetland	1832	691
	Upland	953	1524

Error Matrix	Omission Errors	Commission Errors	Correct
Wetland	27.4%	34.2%	72.6%
Upland	38.5%	31.2%	61.5%
Overall	32.9%	32.9%	67.1%

d. Fuzzy c-means clustering and maximum membership classifier

Contingency Table		Image	
		Wetland	Upland
Ground Truth	Wetland	1561	949
	Upland	562	1928

Error Matrix	Omission Errors	Commission Errors	Correct
Wetland	37.8%	26.5%	62.2%
Upland	22.6%	33.0%	77.4%
Overall	30.2%	30.2%	69.8%

Table 6. October 1 flight – random window comparison

a. Supervised clustering, Bayesian classifier

Contingency Table		Image	
		Wetland	Upland
Ground Truth	Wetland	1473	1005
	Upland	766	1756

Error Matrix	Omission Errors	Commission Errors	Correct
Wetland	40.6%	34.2%	59.4%
Upland	30.4%	36.4%	69.6%
Overall	35.4%	35.4%	64.6%

b. ISODATA clustering, Bayesian classifier

Contingency Table		Image	
		Wetland	Upland
Ground Truth	Wetland	1355	1202
	Upland	668	1775

Error Matrix	Omission Errors	Commission Errors	Correct
Wetland	47.0%	33.0%	53.0%
Upland	27.3%	40.4%	73.7%
Overall	37.4%	37.4%	62.4%

Table 6. (cont'd)

c. Statistical clustering, Bayesian classifier

Contingency Table		Image	
		Wetland	Upland
Ground Truth	Wetland	1437	1039
	Upland	661	1863

Error Matrix	Omission Errors	Commission Errors	Correct
Wetland	42.0%	31.5%	58.0%
Upland	26.2%	35.8%	73.8%
Overall	34.0%	34.0%	66.0%

d. Fuzzy c-means clustering and maximum membership classifier

Contingency Table		Image	
		Wetland	Upland
Ground Truth	Wetland	1393	1116
	Upland	468	2023

Error Matrix	Omission Errors	Commission Errors	Correct
Wetland	44.5%	25.5%	55.5%
Upland	18.8%	35.6%	81.2%
Overall	31.7%	31.7%	68.3%

DISCUSSION

Image Description

A visual examination of the 3-band false color imagery in Figures 4-6 reveals spatial patterns which correspond well with habitat designations on the ground truth map (Figure 13). In all the imagery, the reddish areas associated with greater vegetational biomass generally follow the wetland designations while the bluish colors associated with lesser biomass areas follow the upland designations. This coloration arises because the greater biomass areas reflect a greater portion of the infrared than lesser biomass areas. Because the infrared information is shown in the red portion of the standard red-green-blue (RGB) of color imagery display, the greater biomass appears redder than the lesser biomass imagery, which takes on a bluish or blue-greenish appearance relative to the greater biomass vegetation. The expected phenological changes in the plant communities are manifested by lesser biomass wetland areas as evidenced by the diminished red intensity of the July 22 imagery compared to the June imagery. This is easily seen by a comparison of the center and the lower left edge of the imagery between the June and July periods where the denser vegetation is already dying back as the midsummer conditions affect the moisture sensitive wetland plants. This results in the diminished intensity in the red colors of the imagery. In the October imagery, almost all the denser vegetation has

undergone senescence and appears as brownish areas within the imagery. The open water marsh area at the lower right edge of mosaics has reddened between the June and July imagery, probably due to a combination of denser emergent vegetation and lowering water levels. By October, this same area exhibits virtually no characteristics expected from open water and the emergent vegetation has died back, as evidenced by the lack of enhanced red intensity.

Results of this study indicate that the spectral differences associated with the temporal variation over the sequence of flight dates for specific features can influence classification results due to the influence of timing on these features. As will be noted below, a major problematic area in terms of concurrence between the results based on the classification techniques and the nature of the ground-based delineation process is the disturbed land in the lower or southerly portion of the imagery. Disturbed land area classification is most often affected by the subjective experience of the wetland scientist, whereas the nature of the jurisdictional interpretive process allows interpretations based on normal or expected conditions rather than those actually present.

Overall Study Performance

The overall classification accuracies for all algorithms tested ranged between 60-75% (see Tables 1-6) using analysis of data from a single date.

This compared favorably with the other results based on larger spatial resolution using aircraft MSS (40 m resolution, 68% accuracy, for wetland classifications, Butera [1979]). Improved classification accuracy may be achieved by combining multiple temporal imagery during the classification procedures (Jensen et al., 1986; Jensen et al., 1993b). However, this approach was not attempted as part of this study.

The heavy cloud shadowing a part of the upland area in the southwestern portion of the site on the July overflight (lower left corner of the images) was problematic due to the affected masking of the brightness values primarily in the near-infrared spectral band. Presence of the cloud shadow precluded classification of features within this area for the July imagery. Classification accuracy within this area was also rated poor on the other flight dates and would probably have been poor for the July date as well.

These lower than typical classification accuracies for this area lowered the overall performance for the June and October flight dates for all methods. If the area had been available for classification from the July imagery, it would have probably affected the performance of the classification techniques to yield lower accuracies than those listed in Tables 5a-5d. This is suggested by an examination of the κ values in Table 8 for July. By arranging the κ in Table 8 by rank, it can be seen that the two greatest values (0.396 and 0.376) are from the July imagery and that three

of the four values for July were above the median. This same problem with the July imagery did not exist for the ground point comparison determination (Table 7) because none of the verification points fell within the cloud shadow area.

As an unfunded study, heavy reliance was made on the data from the jurisdictional delineation. Consequentially, the number and location of ground sample points were not entirely adequate. The nature of jurisdictional delineation by an experienced wetland scientist allows for some subjective judgment in the boundary determinations of specific wetland features. Wetland scientists often minimally sample areas that are obviously wetland or upland and concentrate their samples in more questionable areas, such as transition areas between upland and wetland or in areas which have been disturbed in some way. The accuracies predicted by the ground point accuracy testing (Tables 1-3 and 7) were probably biased to lower accuracy values as the points used were in these marginal or questionable areas. An increase in the number and a randomized spatial location process for the selection of ground points for use in accuracy testing would probably have yielded better results in terms of comparing the two approaches.

Registration of the mosaiced images to an orthophotoquad also presented some challenges. The small scale of the orthophotoquad (1:24000)and lack of distinctive features yielded few distinctive points with

Table 7. Kappa values (κ) and standard deviations (σ_κ^2) for ground point comparison calculated from Tables 1-3

Clustering method	κ (σ_κ^2)		
	June	July	October
Supervised	0.453 (0.022)	0.282 (0.020)	0.243 (0.024)
ISODATA	0.360 (0.022)	0.189 (0.024)	0.028 (0.021)
Statistical	0.342 (0.024)	0.329 (0.024)	0.241 (0.021)
Fuzzy c-means	0.412 (0.022)	0.283 (0.023)	0.360 (0.018)

Table 8. Kappa values (κ) and standard deviations (σ_κ^2) for random window comparison calculated from Tables 4-6

Clustering method	$\kappa(\sigma_\kappa^2)$		
	June	July	October
Supervised	0.368 (0.000173)	0.376 (0.000170)	0.291 (0.000182)
ISODATA	0.293 (0.000183)	0.247 (0.000188)	0.255 (0.000178)
Statistical	0.295 (0.000178)	0.342 (0.000175)	0.319 (0.000176)
Fuzzy c-means	0.348 (0.000176)	0.396 (0.000165)	0.367 (0.000161)

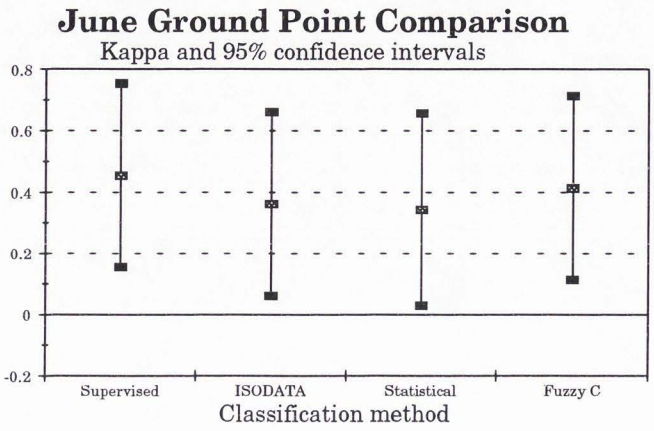

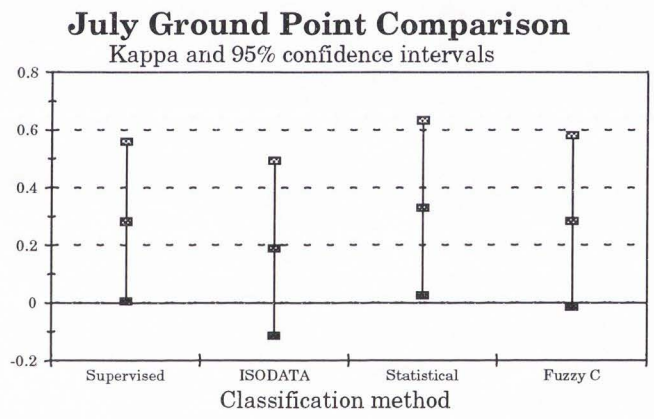

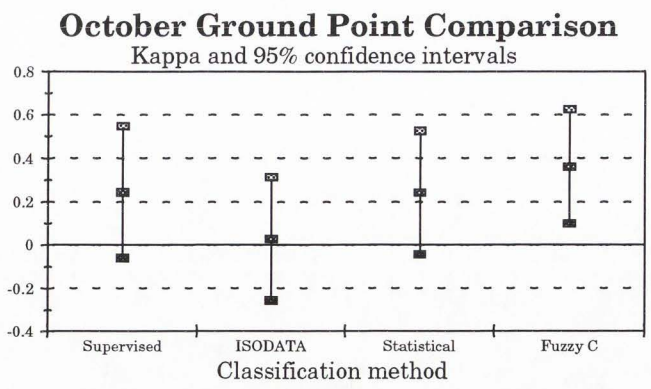

Figure 17. Kappa values and 95% confidence intervals for the ground point comparison for all dates.

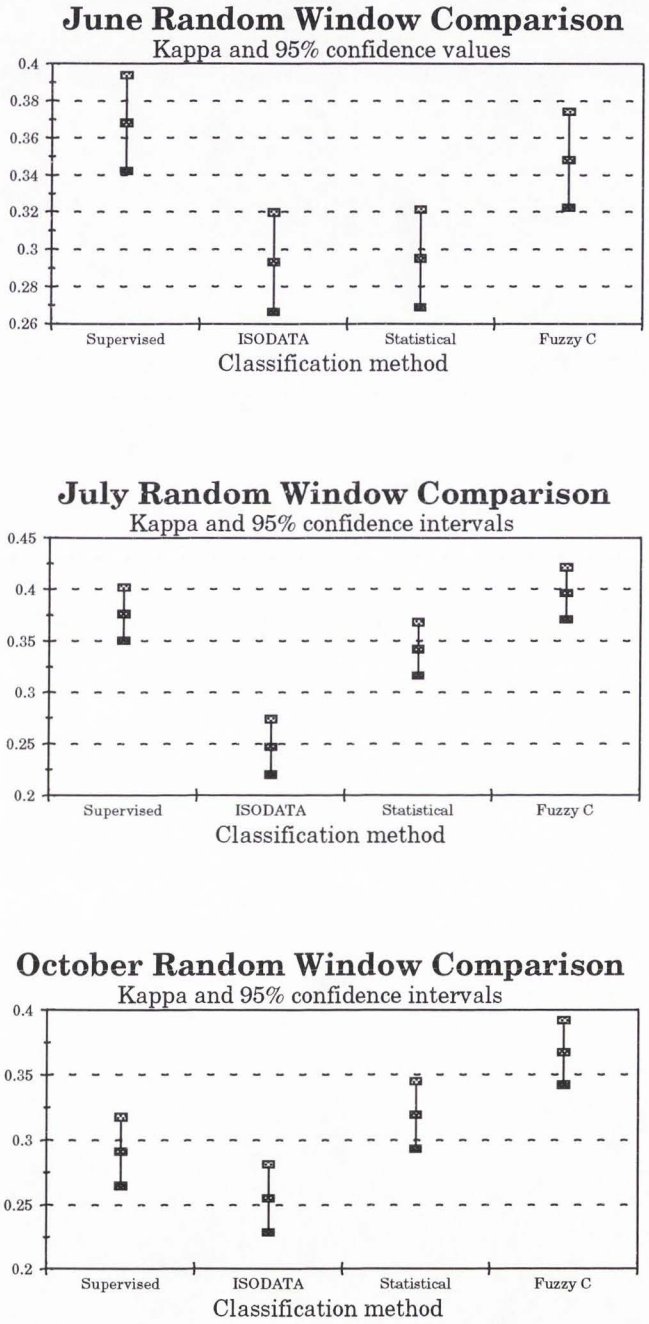

Figure 18. Kappa values and 95% confidence intervals for the random window comparison for all dates.

which to anchor the mosaics. The scale of the orthophotoquad corresponds to almost a 20 m resolution, which is represented by 25 to 35 pixels in the mosaiced images. Also, due to the age of the aerial photographs used for the orthophotoquad, many of the features present in the imagery (e.g., residential roads and buildings, businesses, a golf course on the northwest edge of the site) were not on the orthophotoquad. As a result of the relatively low resolution and lack of common features of the orthophotoquad, registration error was significant enough to preclude the use of the classified images as a map. This registration error also affected the accuracy results derived from the random window accuracy testing and most probably resulted in underestimating the actual accuracies.

One objective of this research was to determine the temporal effects on classification. Two factors significantly hampered acquiring the requisite data for completely achieving this objective. At the time of this work, an easily applied and suitable method for radiometric correction of the imagery for each of the flights was not available. This precluded the direct comparison of radiometric values between images of successive dates to determine the temporal effects on the area of interest in terms of radiometric response in the vegetational elements.

The second shortcoming was the lack of data from early spring (late April to early May), which would have allowed a more detailed study of the phenological responses of the plant communities. Delay in image

acquisition was due to Federal Aviation Administration (FAA)-required modifications to the sensor platform. In this region, upland grasses typically grow quickly in the early spring in order to take advantage of the relative abundance of water at this time of year. By early summer, much of this upland grass growth has gone into senescence and the wetland/riparian vegetation, which has a more reliable source of water, begins to dominate. Other researchers have found a greater ability to differentiate wetlands by taking advantage of differences in the phenological cycle (Jensen et al., 1986; Jensen et al., 1993b). Although the visual differences in the images from the June and July dates are not great, it is interesting to note that the June date had the highest classification accuracies of all dates for the wetland class. The use of radiometrically corrected data sets collected from early spring through late summer might enhance the accuracy of the classification, by better identifying upland vegetation as well as providing important monitoring of seasonal changes.

The potential usefulness of an earlier flight can be seen in the estimated areas of wetland hectares in Table 9. The decreasing values of wetland area (or as a percentage of the total area) are indicative of the seasonal variation in water supply for this area and its effect on the phenology of the plant communities. For the jurisdictional delineation by the Corps, wetland area is a constant because the delineation is based on the maximum wetland area independent of seasonal variation as

incorporated by the phrase "normal circumstances" in the legal definition. Clearly, the interaction between phenological responses of the vegetation to site specific hydrology and timing of remotely acquired data shows a temporal variation in study results, which in turn can result in significant differences in the amount of area associated with wetlands at a specific site.

Differential results in wetland area classifications have direct implications from a legal or institutional framework. The size of the distinguished areas from any delineation process directly affects the nature and extent of permitted activities based on the regulations governing wetlands. This is further compounded by the shifting definition for jurisdictional wetlands and suggests that results based on analyses of multispectral videography from a number of representative wetlands over time could be used by wetland scientists to make the criteria for wetland definition more objective.

Classifier Performance

Visual evaluation

Supervised clustering. Supervised clustering used with the Bayesian/ maximum likelihood classifier produced results in which both wetland and upland areas showed good correspondence to the boundaries of these classes in the jurisdictional delineation. A visual comparison of the classification results provided in Figures 10a, 11a, and 12a against the ground-based

Table 9. Wetland area in hectares and as a percentage of the total area

	Flight Date		
	June	July	October
Supervised clustering	23.76 ha	21.29 ha	20.42 ha
	51.50%	46.41%	45.49%
ISODATA	25.53 ha	23.77 ha	19.09 ha
	54.61%	52.28%	41.63%
Statistical clustering	26.69 ha	25.39 ha	19.55 ha
	57.40%	56.32%	43.33%
Fuzzy c-means	24.07 ha	19.87 ha	16.30 ha
	51.45%	43.49%	36.50%
Ground truth	25.56 ha		
	49.71%		

delineation map in Figure 13 shows that the boundaries for both the upland and wetland classes are in close agreement for the June flight, with progressively worse performances for the later dates. As mentioned previously, the disturbed lands located in the lower left-hand area of the imagery have the lowest classification accuracy of any portion of the imagery for all flight dates as compared against the ground-based delineation. This is evident by visual inspection of the classified imagery and ground based delineation map. In the June imagery, the disturbed area contains a mix of wetland/upland classes, while in the July imagery

the wetland classified areas decrease dramatically. In the October imagery, this disturbed area is almost entirely classed as upland. Other portions of this imagery show the same progression, but not to the same extent. The differential classification of wetland versus upland in the videography reflects this phenological change while the ground-based classification does not. The resulting lower classification accuracy for this area is attributed to the static delineation based on the subjective professional judgment of the wetland scientist in delineation of wetland and upland features in this disturbed land area versus the reliance only on vegetational and surface soil spectral properties for the video-based classifications.

ISODATA clustering. A visual comparison of the ISODATA clustering results is provided in Figures 10b, 11b, and 12b. As can be seen, this algorithm generally does a poor job in representing the spatial relationships of wetland and upland features compared to the ground-based delineations in Figure 13. In particular, notice the "speckling" pattern of classified features evident in all the classified imagery, which is especially evident in the July results. This is in contrast to the results presented above for the supervised classification results. In general, classification results for ISODATA are the poorest compared for all sampling dates when compared with other classification techniques employed in this study. However, ISODATA does show a reduction in the wetland class areas over the period of sampling dates, as was observed in the supervised clustering

results discussed above. As was noted for the supervised clustering results, ISODATA also shows the poorest performance in the disturbed land area in the lower left portions of the imagery during all sampling dates.

Statistical clustering. Statistical clustering results are presented in Figures 10c, 11c, and 12c. A visual inspection of these results shows that this algorithm performed better than the ISODATA clustering but was not as good as the supervised clustering approach. In general, the statistical clustering can be seen to have overclassified wetland features during June compared to the ground-based delineations shown in Figure 13. Overclassification of wetlands is also evident in the upper portions of the imagery for the July date, but is generally close to the delineated wetland features in this area of the imagery for the October data. Under-classification of wetlands in October, however, is evident in the lower portion of the imagery. As was noted for the other algorithms, statistical clustering of vegetational features is poorest in the disturbed land areas when compared against the ground-based delineations located in the lower left portions of the imagery on all flight dates. The statistical clustering approach also shows a reduction in wetland area classifications over the time sequence of the imagery, reflecting the phenological changes evident in the plant communities.

Fuzzy c-Means. Results for the fuzzy c-means classification results for all three time periods are provided in Figures 10d, 11d, and 12d.

Comparison of these images with the ground-based delineations in Figure 13 shows that, in general, this approach represents the spatial characteristics of the vegetation classes for all three flight dates and is similar in this regard to the supervised classification results shown in Figures 10a, 11a, and 12a. This similarity to the supervised results is demonstrated in Figure (19) for the June imagery where the fuzzy c-means results are overlaid on the results from the three parametric techniques. The figure also shows some of the speckling of the ISODATA method and a tendency of the statistical clustering to overclassify for wetlands in the center of the image.

A careful examination of the results for the June fuzzy c-means shows an overclassification of wetland features in the upper area of this imagery as seen on the ground truth map. The results in July show some improvement in this regard for the upper area, but show underclassification of wetland features in the lower areas of the July imagery. The October classification shows some problems along the right-hand side of the imagery (east side) as exhibited by a marbled appearance in the wetland classes due to misclassification of some wetland from the ground-based delineation as upland. As was noted for all classification approaches, fuzzy c-means results are poorest in the disturbed land areas when compared against the ground-based delineation of features in this area. Fuzzy c-means

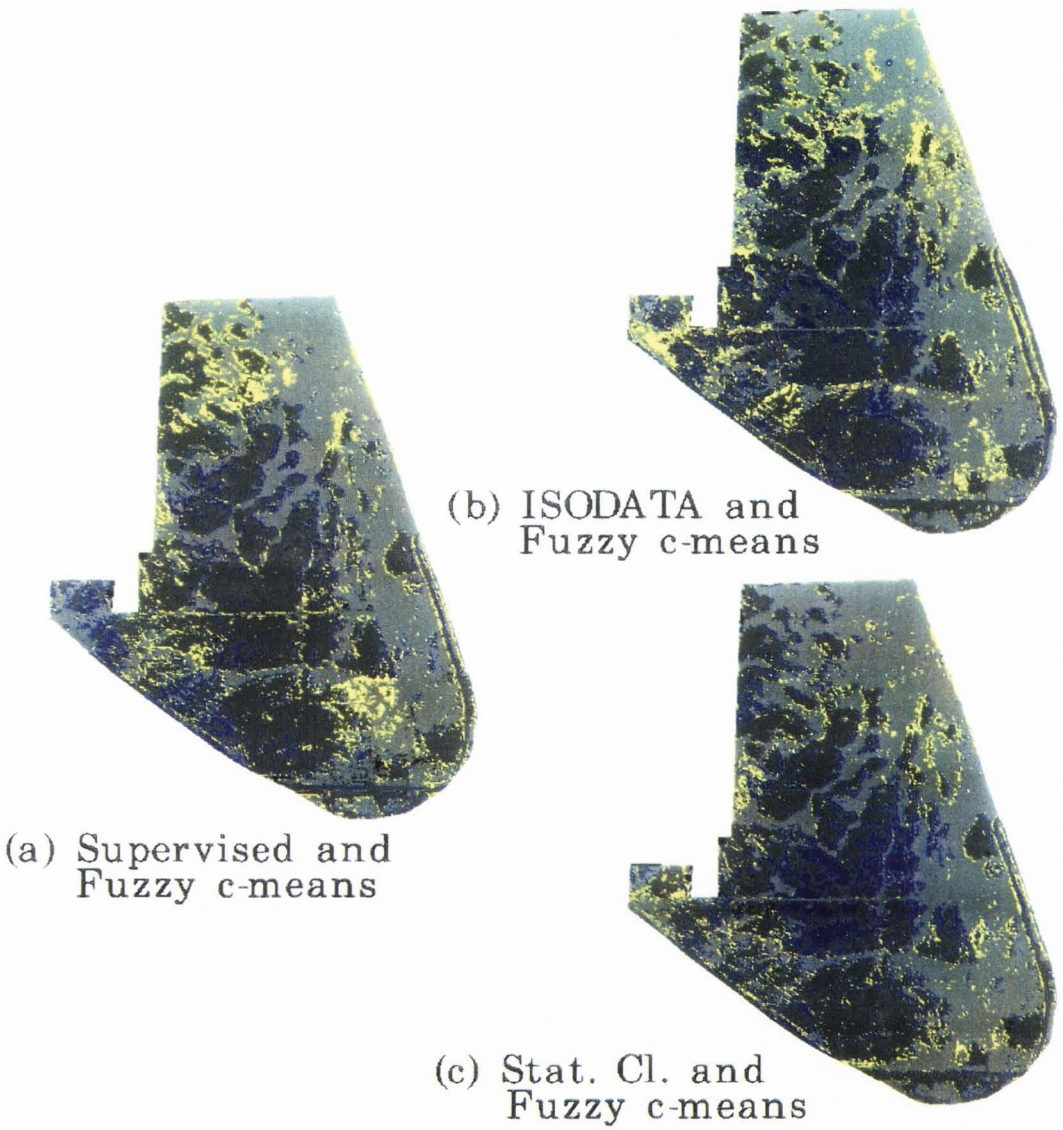

Figure 19. June flight date Fuzzy c-means overlaid on all three parametric techniques. (key: Dk gray - upland/both; Lt Gray - wetland/both; Blue - upland/Fuzzy, wetland/parametric; Yellow - wetland/Fuzzy, upland/parametric)

classification results also show a consistent reduction in the area associated with wetland features over the time period of imagery.

Performance based on ground point comparison

A quantitative assessment of classification accuracy for each of the algorithms was made based on comparison of ground points from the ground truth map to classified features (see Figure 9 and Results section above). It should be remembered that a limited number of ground points were available for this study and that algorithm performance characteristics may have been biased by both the small sample size and spatial location of the ground points.

The κ values in Table 7 show that algorithm performance based on ground point comparisons is highly dependent on date-of-flight acquisition. The κ values within each flight date were submitted to the χ^2 test discussed in the Materials section above. The null hypothesis of equal κ's was not rejected. An examination of the 95% confidence intervals from Figure 17 shows significant overlap of the κ values in Table 7. Because the variance as calculated in equation (14) is proportional to 1/N, the small sample size results in large confidence intervals. As a consequence, only general inferences about the performance of the algorithms as tested with the ground point comparison can be made.

For the June results, the supervised classification approach shows the best overall performance. The fuzzy c-means algorithm has similar performance to the supervised clustering approach when compared with the other algorithms tested. The results for July show that the best algorithm performance is achieved using statistical clustering. As in June, the results for supervised clustering and fuzzy c-means are similar in July. Fuzzy c-means results in October produced the best performance using the ground point comparisons. Supervised clustering and statistically clustering approaches are very similar for this date.

Study results indicate that the ISODATA clustering/Euclidean classifier is the poorest of all the classification techniques. This is pointedly illustrated by the October κ of 0.028 in Table 7, which indicates the ISODATA technique is no better than a random assignment of ground-based points on this date. This is supported by the random speckling of the classification discussed above. For the July date it is the poorest performer and had one of the lowest κ values for the June date.

The results in Table 7 show a trend toward generally poorer performance with later flight dates and this trend is reflected in the results for all methods. This is expected from the normal drop in wetland vegetation cover and density during the lower water levels at midsummer and is further supported by other researchers who have found that earlier

dates in the growing season result in greater accuracy for wetland classification (Jensen et al., 1987).

Performance based on random window comparisons

An alternative assessment of algorithm performance based on a comparison of classification results with the ground-based delineations was conducted by use of a 5-by-5 randomized window as described above. This approach was undertaken due to concerns of the low number of ground points available and spatial bias noted in the previous section.

The κ values in Table 8 show that algorithm performance based on a randomized window comparison is highly dependent on date-of-flight acquisition as was found for the ground point comparison results noted above. The χ^2 test for the κ values from the randomized window comparison rejects the null hypothesis of equal κ's. The 95% confidence intervals are plotted in Figure (18). The larger sample size (5000 vs. 38 for the ground point comparison) helped narrow the confidence intervals such that meaningful compaisons could be made between methods. Results for June indicate that the supervised clustering approach performed best in agreement with the indication from the ground point comparison. Additionally, as was suggested by the ground point results for this date, the fuzzy c-means algorithm is similar to the supervised classification approach. The results for July also show that the fuzzy c-means and supervised

clusterring algorithms are the best with a slight edge to fuzzy c-means. The statistical clustering results are slightly worse than the supervised clustering results and statistically lower than the fuzzy c-means. Results for October show that the fuzzy c-means algorithm is again the best based on this test. The fuzzy c-means shows strong superiority over other methods for this late season flight. The supervised clustering and statistical clustering approach are similar, with a slight edge to the statistical clusterring algorithm. As suggested by the ground point comparisons, the ISODATA clustering results are overall the poorest when compared to all other approaches.

Overall Algorithm Rating

In general, both testing procedures examined to assess algorithm performance show that either the supervised clustering or fuzzy c-means approaches are superior to other methods examined. The only exception is the better performance indicated by the ground point measurement test for the July imagery, where statistical clustering is found to perform better than these other two techniques. Caution must be exercised, however, in reliance on the ground-based test procedures given the limited number of sample points and poor representation of vegetational features throughout the spatial area covered by the imagery.

The poor performance of ISODATA is attributed to two weaknesses in the technique as compared to the other methods. The Euclidean classifier disregards within-cluster variability and so assumes that all clusters have the same variability. Thus, for a class with high variability, members that should fall within the class, but are at the edges of the "cluster space," will instead be placed in a neighboring cluster. The Bayesian/maximum likelihood classifier used by the supervised and statistical clustering algorithms does not have this shortcoming because it considers within-cluster variability in its classification. The second weakness is the method of initial cluster center selection of the ISODATA algorithm. The selection of cluster centers along the principal axis of the data set biases the final cluster centers along this axis. A visual examination of the two-dimensional projections of the final ISODATA clusters for most images shows them to be a series of stacked discs (similar to stacked dinner plates) oriented along the principal axis. This principal axis generally falls along the soil line (Jackson, 1983). This line is used as a starting point for the perpendicular vegetation index (PVI) used in predicting the biomass (e.g., grams of plant mass per square meter) of a natural system. This is valuable information for predicting the type and health of vegetation. The orientation of the clusters is parallel to the information contained in the PVI, so this valuable information is suppressed. Based on these factors and study results, ISODATA is judged to be inferior compared to other approaches and

is probably not suitable for applications of wetland delineations under similar study conditions. No other specific reference in the literature was found for the successful application of this particular clustering technique for wetland delineations.

The statistical clustering method is found to be the best classifier for the July data using the ground point testing procedure, and generally performs similar to the supervised classification approach for other flight dates. This is attributed to the use of the Bayesian/maximum likelihood classifier by the statistical clustering technique which allows it to approach the performance of the supervised clustering method. Other factors which may have contributed to its generally good performance are related to the operator selection of the criteria for use in homogeneity testing as discussed in the Material and Methods section. This can allow the algorithm to define a fairly narrow definition of spectral properties associated with clusters and therefore produce similarly narrow clusters as derived from supervised signature extraction techniques. One disadvantage to this algorithm is its bias towards classes in the top left corner of the image since it only uses a single linear pass through the file, starting in the upper left corner and working horizontally to the lower right corner. This drawback could present problems if used in other classification studies.

The supervised classification approach does provide the best performance among the parametric methods when all dates are considered

(i.e., excluding the fuzzy c-means results). In comparison to the other parametric methods, the narrow definition of each class afforded by operator supervision allows more refined clustering. Coupled with the Bayesian/maximum likelihood classifier, this provides the overall highest accuracy among the parametric techniques. A disadvantage of the supervised clustering approach is related to the operator intensive nature of this approach during signature extraction and class definitions. This approach also relies heavily on either ground-based measurements or ocular interpretation of image features in the class selection process.

The only nonparametric method tested in this study is the fuzzy c-means algorithm. Compared to the other classification procedures, and in particular the supervised clustering approach, fuzzy c-means requires the least operator interaction. Typical processing time is a few hours to cluster, classify, and perform accuracy evaluation of the preprocessed imagery. This compares to one (unsupervised) to several days (supervised) for the parametric methods. Another advantage of the fuzzy c-means classification method is its ability to classify pixels as having partial membership in all defined clusters for a particular image. This property was not exploited in this study but may have importance in the delineation of transitional areas where mixed features may have both physical and biological significance for the investigator. Fuzzy c-means classification can also be used to exploit non-Euclidian distance metrics as well as allowing nonellipsoid cluster

shapes in the classification procedures. Traditional classification algorithms use class parameters (mean, standard deviation, etc.) to specify the shape of the class and force the data to conform to this shape, typically ellipsiodal (in three dimensions). Shape adaptive fuzzy-c algorithms are available which can "find" cluster shapes within the data set whether cluster are ellipsoidal, linear or a combination of these shapes or others. This may be a significant advantage for some types of data where cluster shape is markedly nonellipsoidal (Gunderson, 1983).

Although the supervised, and to a lesser degree the statistical, clustering approaches are generally similar to the fuzzy c-means results, based on the factors discussed above, the fuzzy c-means approach is judged to be the best algorithm for use in wetland delineations for this study.

SUMMARY

The overall accuracies in the range of 60-80% were comparable to those found using smaller scale techniques as described in the literature. The supervised clustering provided the best performance, but with a significant increase in time required. From Table 10 and Figure 20 it is obvious that the unsupervised methods can probably give the desired accuracy in most cases with significant reduction in processing time. High altitude aerial photography is the most widely used method for wetland identification, and though it can provide the necessary spatial accuracy, it is hampered by difficulty in digitization and sometimes poor spectral resolution (Carter, 1982; Jensen et al., 1993b).

Table 10. Time estimates for major phases of the project

Category	Time (hours)
Image digitization	7
Image preprocessing	75
Supervised clustering	75
ISODATA clustering	25
Statistical clustering	25
Fuzzy C-means	10

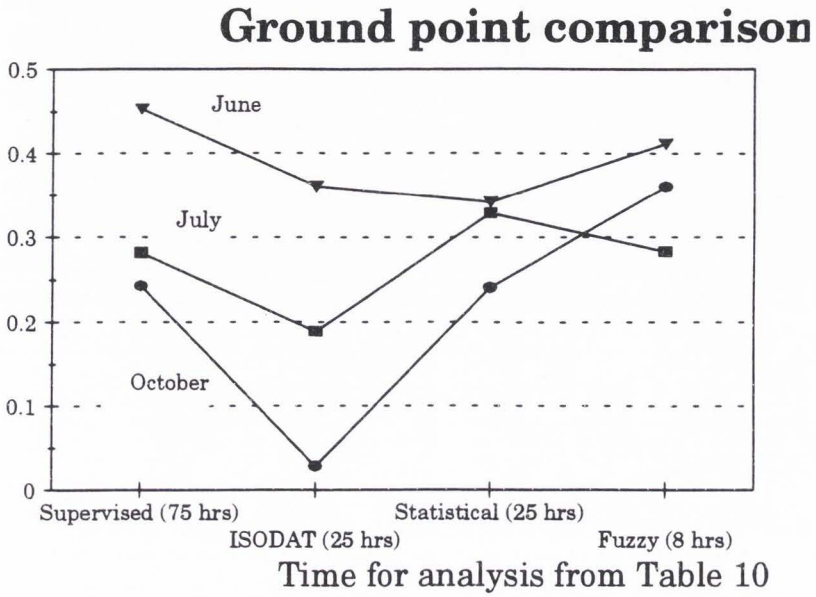

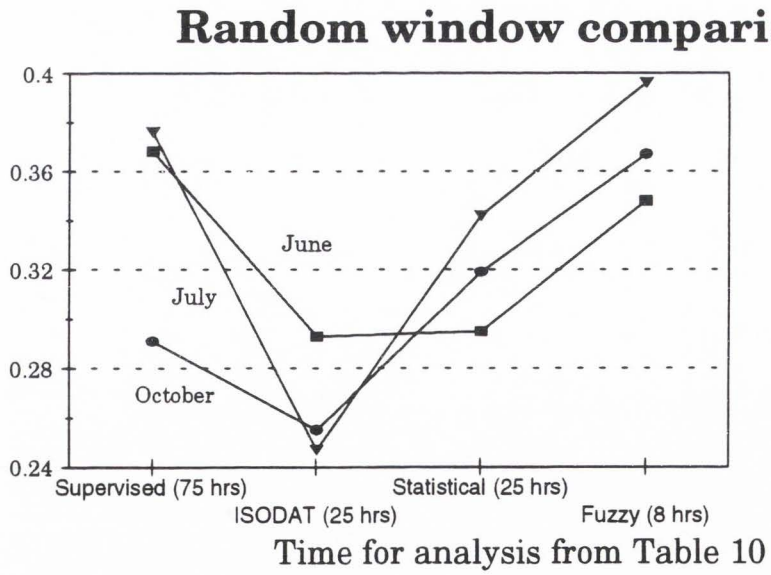

Figure 20. Plot of kappa for each algorithm by date versus estimated processing time.

The fuzzy c-means clustering was the best of the unsupervised methods. Its κ values in Tables 7 and 8 exceeded all but the July statistical clustering ground point comparison. The performance of the fuzzy c-means classifier can most probably be attributed to superior performance for mixed pixels at transition regions. As this technique receives further use, its performance will undoubtedly improve. One of the pieces of information provided by the fuzzy c-means method, absent in the parametric techniques, is data about the sample's relationship to all classes. A limitation for this study was the inability to present fuzzy data in viewable form. The use of operator-provided training sets could also make it measurably better than the supervised classifier. When a technique is developed to exhibit not only the fuzzy cluster, to which the sample most strongly belongs, but also information about the strength of that and other cluster relationships, then fuzzy sets may indeed replace parametric techniques in most applications.

Overall, a visual examination of conventional ground-based maps (NWI, US Geological Survey 1:24000) such as standard 1:24000 quad maps shows the classified images to be more accurate in identification of wetland areas. This application demonstrated the usefulness of multispectral videography in jurisdictional delineation of wetland areas, although it is still dependent on some minimal ground-based sampling. Multispectral videography in the form of unsupervised classified imagery could also prove

valuable as a field tool to improve classification and boundary determination by the wetland scientist.

Two important uses will arise from the development of successful aerial videography techniques for wetland mapping. Natural resource managers can monitor wetlands and examine temporal changes associated with usage impact, rehabilitation, and natural processes. Additionally, spatially accurate and reproducible quantification of wetland boundaries, whether for jurisdictional delineation or other uses, promises to aid in the protection of these vital areas. The Corps processes over 15,000 permit applications each year involving dredge and fill of wetlands (Want, 1989). A jurisdictional delineation survey accompanies each application. An often critical part of the permit process is the determination of the wetlands area. Because of the 1- and 10-acre breakpoints, changes are triggered in permit handling procedures. Because of the advantage provided by the inexpensive high-spatial resolution from digital video imagery, the successful application of this technique can aid in a timely evaluation of wetland sites. These results can be used in the planning stage to minimize potential impact and aid resource managers and engineers in better system design and long-term trend monitoring based on quantifiable and repeatable data within a GIS framework.

RECOMMENDATIONS

A number of improvements and areas of further study come to mind. As previously mentioned, a greater number of ground points to improve statistical comparisons are desirable. A more suitable sampling scheme would be to select sample points based on some type of gridded pattern or stratified random sampling. In addition, a much greater number of sample points would be needed for accuracy testing. Work by Hord and Brooner (1976) and Schowengerdt (1983) has suggested that as many as 250 points might be needed for accuracy estimates with 95% confidence levels.

Concurrent with an increase in the number of ground sample points, an improvement in fixing the location of these points is needed. To improve determination of sample point location, a hand-held GPS unit could be used to reduce image rectification error. This would reduce the problem with error due not to misclassification, but instead due to misrectification. In addition, differential GPS would allow the use of the classified mosaic as a planimetrically accurate layer in a geographic information system (GIS).

Another improvement would be the development of easily applied techniques for radiometric correction of the video data. This would allow the direct comparison of image brightness values between dates using a normalized scale. This approach could be used along with differences in the phenological cycles of wetland and upland to test the ability of differing time-of-season flights in enhancing the accuracy of the classification.

An interesting separate study would be improvements or modifications to the fuzzy sets technique. One immediate improvement would be the use of alternative distance algorithms. Measurements such as the Mahalanobis measurement, which incorporate within-cluster variation, could improve the identification of marginal cluster members. Another improvement would be the use of shape-adaptive algorithms suggested by Gunderson (1983). Use of such an algorithm would allow the fuzzy clustering techniques to find nonspherical clusters. In addition, user-supplied training sets, along with the radiometrically corrected imagery in a semisupervised approach, could be used to monitor areas as they shift from one group to another. This could give quantifiable indications of improvement or degradation of a wetland area.

ENGINEERING SIGNIFICANCE

The interest in identifying and monitoring wetlands will continue to increase as such areas are subjected to the often competing pressures of development and conservation. To meet these goals, the resource manager, politician, conservationist, businessperson, and other interested parties require quick, cheap, and accurate multipurpose tools. With accuracies as good or better than conventional methods, and the advantage of its digital nature, multispectral videography has demonstrated its ability to fulfill these requirements.

Multispectral videography can provide direct input to digital mapping databases. This input can be displayed along with other geographic information to allow informed and objective data for decisions affecting these areas. Incorporation with radiometric information will allow comparison between different dates for data collection. The timely nature of data collection and ease of its analysis, when compared with conventional techniques, means that data can be collected at shorter intervals. By having more rapid feedback, the outcomes of these management decisions can be monitored and corrective actions taken more quickly to reduce any adverse effects.

REFERENCES

Bartlett, D.S., and V. Klemas. 1980. Quantitative assessment of tidal wetlands using remote sensing. Environmental Management 4(4):337-345.

Bezdek, J.C., C. Coray, R. Gunderson, and J. Watson. 1981. Detection and characterization of cluster substructure - I. Linear structure: Fuzzy c-lines. SIAM Journal of Applied Mathematics 40(2):339-357.

Bishop, Y.M.M., S.E. Fienberg, and P.W. Holland. 1975. Discrete multivariate analysis: Theory and practice. The MIT Press, Cambridge, Massachusetts. 557 p.

Blazquez, C.H. 1988. Use of aerial color infrared photography, dual color video, and a computer system for property appraisal of citrus groves. Photogrammetric Engineering and Remote Sensing 54(2):233-236.

Bukata, R.P., J.E. Bruton, and J.H. Jerome. 1983. Use of chromaticity in remote measurements of water quality. Remote Sensing of Environment 13:161-177.

Bukata, R.P., J.H. Jerome, and J.E. Bruton. 1988. Relationships among secchi disk depth, beam attenuation coefficient, and irradiance attenuation coefficient for great lake waters. Journal of Great Lakes Research 14(3):347-355.

Bukata, R.P., J.H. Jerome, J.E. Bruton, and E.B. Bennett. 1978. Relationship among optical transmission, volume reflectance, suspended mineral concentration, and chlorophyll *a* concentration in Lake Superior. Journal of Great Lakes Research 4(3-4):456-461.

Butera, M.K. 1979. Demonstration of wetland vegetation mapping in florida from computer-processed satellite and aircraft multispectral scanner data. NASA Technical Paper 1553. 19 p.

Campbell, J.B. 1987. Introduction to remote sensing. Guilford Press, New York. 551 p.

Carter, V. 1982. Applications of remote sensing to wetlands, p. 284-300. In Remote sensing for resource managers. C. J. Johannsen and J. L. Sanders (Ed.). Soil Conservation Society of America, Ankena, Iowa.

Cohen, J. 1960. A coefficient of agreement for nominal scales. Educational and Psychological Measurement XX(1):37-46.

Crowther, B. 1992. Radiometric calibration of multispectral video imagery. Unpublished MS thesis. Utah State University Library, Logan, Utah. 119 p.

Crowther, B.G., and C.M.U. Neale. 1991. Calibration of multispectral video imagery, p. 51-59. In Automated agriculture for the 21st century: proceedings of the 1991 symposium. American Society of Agricultural Engineers, Chicago, Illinois.

Dahl, T.E., and C.E. Johnson. 1991. Status and trends of wetlands in the conterminous united states, mid-1970's to mid-1980's. U.S. Department of the Interior, Fish and Wildlife Service, Washington, D.C. 28 p.

Dottavio, C.L., and F.D. Dottavio. 1984. Potential benefits of new satellite sensors to wetland mapping. Photogrammetric Engineering and Remote Sensing 50(5):599-606.

Duda, R.O., and P.E. Hart. 1973. Pattern classification and scene analysis. John Wiley & Sons, New York. 482 p.

Environmental Laboratory. 1987. Corps of engineers wetlands delineation manual, technical report y-87-1. US Army Engineer Waterways Experiment Station, Vicksburg, Mississippi.

ERDAS. 1991. ERDAS field guide. 2nd edition, version 7.5. ERDAS, Inc., Atlanta, Georgia. 394 p.

Everitt, J.H., D.E. Escobar, M.A. Alaniz, and M.R. Davis. 1987. Using airborne middle-infrared (1.45-2.0 um) video imagery for distinguishing plant species and soil conditions. Remote Sensing of the Environment 22:423-428.

Everitt, J.H., D.E. Escobar, M.A. Alaniz, and M.R. Davis. 1989. Using multispectral video imagery for detecting soil surface conditions. Photogrammetric Engineering and Remote Sensing 55(4):467-471.

Everitt, J.H., D.E. Escobar, A.H. Gerbermann, and M.A. Alaniz. 1988. Detecting saline soils with video imagery. Photogrammetric Engineering and Remote Sensing 54(9):1283-1287.

Everitt, J.H., D.E. Escobar and P.R. Nixon. 1987. Near-real-time video system for rangeland assessment. Remote Sensing of the Environment 23:291-311.

Everitt, J.H., D.E. Escobar, R. Villarreal, J.R. Noriega, and M.R. Davis. 1991. Airborne video system for agricultural assessment. Remote Sensing of the Environment 35:231-242.

Everitt, J.H., and P.R. Nixon. 1985. False color video imagery: A potential remote sensing tool for range management. Photogrammetric Engineering and Remote Sensing 51(6):675-679.

Fleiss, J.L. 1981. Statistical methods for rates and proportions. Second edition. John Wiley & Sons, New York. 321 p.

Foody, G.M. 1992. A fuzzy sets approach to the representation of vegetation continua from remotely sensed data: an example from lowland heath. Photogrammetric Engineering & Remote Sensing 58(2):221-225.

Grah, O., and J.E. Crane. 1991. Jurisdictional wetlands inventory and mapping for Farmington City, Utah. Ecotone Environmental Consulting, Inc., Logan, Utah. 30 p.

Gunderson, R.W. 1983. An adaptive FCV clustering algorithm. International journal for man-machine studies. 19:97-104.

Gunderson, R.W. 1994. Professor of Electrical Engineering, Utah State University. Personal interview, April 13.

Gunderson, R.W., and T. Jacobsen. 1983. Cluster analysis of beer flavor components. I. Some new methods in cluster analysis. American Society of Brewing Chemists Journal 41(2):73-77.

Hook, D.D. 1986. Volume 1: Ecology of wetlands. Timber Press, Portland, Oregon. 592 p.

Hord, R.M., and W. Brooner. 1976. Land-use map accuracy criteria. Photogrammetric Engineering and Remote Sensing 42(5):671-677.

Jackson, R.D. 1982. Canopy temperature and crop water stress, p. 43-85. In Advances in irrigation. D. Hillel (Ed.). Academic Press, New York.

Jackson, R.D. 1983. Spectral indices in n-space. Remote Sensing of Environment 13:409-421.

Jensen, J.R., D.J. Cowen, J.D. Althausen, S. Narumalani, and O. Weatherbee. 1993a. An evaluation of the coastwatch change detection protocol in South Carolina. Photogrammetric Engineering and Remote Sensing 59(6):1039-1046.

Jensen, J.R., M.E. Hodgson, E. Christensen, H.E. Mackey, L.R. Tenney, and R. Sharitz. 1986. Remote sensing inland wetlands: A multispectral approach. Photogrammetric Engineering and Remote Sensing 52(1):87-100.

Jensen, J.R., S. Narumalani, O. Weatherbee, and J. H.E. Mackey. 1993b. Measurement of seasonal and yearly cattail and waterlily changes using multidate SPOT panchromatic data. Photogrammetric Engineering and Remote Sensing 59(4):519-525.

Jensen, J.R., E.W. Ramsey, H.E. Mackey, E.J. Christensen, and R.R. Sharitz. 1987. Inland wetland change detection using aircraft MSS data. Photogrammetric Engineering and Remote Sensing 53(5):521-529.

Johnson, R.W., and R.C. Harriss. 1980. Remote sensing for water quality and biological measurements in coastal waters. Photogrammetric Engineering and Remote Sensing 46(1):77-85.

Kentula, M.E., J.C. Sifneos, J.W. Good, M. Rylko, and K. Kunz. 1992. Trends and patterns in section 404 permitting requiring compensatory mitigation in Oregon and Washington, USA. Environmental Management 16(1):109-119.

King, D., and J. Vlcek. 1988. Multispectral Video Image Characteristics and their Application in Land Cover Classification. 13 p. In Videography: first workshop held at Tirey Memorial Union, Indiana State University, Terre Haute, Indiana. American Society of Photogrammetry, Falls Church, Virginia.

King, D. and J. Vlcek. 1990. Development of a multispectral video system and its application in forestry. Canadian Journal of Remote Sensing 16(1):15-22.

Klemas, V., M. Otley, W. Philpot, C. Wethe, R. Rogers, and N. Shah. 1974. Correlation of coastal water turbidity and current circulation with ERTS-1 Skylab imagery, p. 1289-1317. In Proceedings of the ninth international symposium on remote sensing of environment, Environmental Research Institute of Michigan, Ann Arbor, Michigan.

Kuchler, A.W., and I.S. Zonnveld. 1988. Vegetation mapping. Kluwer Academic Publishers, Dordrecht, the Netherlands. 635 p.

Kusler, J. 1992. Wetlands delineation: an issue of science of politics? Environment Vol 34(2):7+.

Lathrop, R.G., Jr., and Thomas M. Lillesand. 1986. Use of thematic mapper data to assess water quality in Green Bay and central Lake Michigan. Photogrammetric Engineering and Remote Sensing 52(5):671-680.

Lulla, K., P. Mausel, D. Skelton and W. Kramber. 1987. An evaluation of video-band based vegetation indices, p. 270-279. In Proceeding of the 11th biennial workshop on color aerial photography and videography in the plant sciences. American Society of Photogrammetry, Falls Church, Virginia.

Lyon, J.G., and I.H.S. Khuwaiter. 1988. Cropland measurement using Thematic Mapper data and radiometric model. Journal of Aerospace Engineering 2(3):130-140.

Marsh, S.E., J.L. Walsh, and C.F. Hutchinson. 1990. Development of an agricultural land-use GIS for senegal derived from multispectral video and photographic data. Photogrammetric Engineering and Remote Sensing 56(3):351-357.

Mausel, P.W., J.H. Everitt, D.E. Escobar, and D.J. King. 1992. Airborne videography: Current status and future perspectives. Photogrammetric Engineering and Remote Sensing 58(8):1189-1195.

Mitsch,W.J., and J.G. Gosselink. 1986. Wetlands. Van Nostrand Reinhold Company Inc., New York. 529 p.

Neale, C.M.U. 1992. An airborne multispectral video/radiometer remote sensing system for natural resource monitoring, p. 119-126. In Proceeding of the 13th biennial workshop on color aerial photography and videography in the plant sciences. American Society of Photogrammetry, Falls Church, Virginia.

Neale, C.M.U., J. Kupier, S. Ram, and K.L. Tarbet. 1993. Image enhancement and processing automation routines for digital multispectral video imagrey. In Proceeding of the 14th biennial workshop on color aerial photography and videography in the plant sciences. American Society of Photogrammetry, Falls Church, Virginia, in press.

Nixon, P.R., D.E. Escobar, and R.M. Menges. 1985. A multiband video system for quick assessment of vegetal conditions and discrimination of plant species. Remote Sensing of the Environment 17:203-206.

Ormsby, J.P., J.C. Gervin, J.E. Nickeson, and G. Wiley. 1985. Wetland physical and biotic studies using multispectral data, p. 799-807. In Proceedings of the nineteenth international symposium on remote sensing of environment, Environmental Research Institute of Michigan, Ann Arbor, Michigan.

Ossinger, M.C., J.A. Schafer, and R.F. Cihon. 1992. Method to identify, inventory, and map wetlands using aerial photography and geographic information systems, p. 35-40. In Transportation research record # 1366, Transportation Research Board, National Research Council.

Rees, W.G. 1990. Physical principles of remote sensing. Cambridge University Press, Cambridge, England. 247 p.

Richardson, A.J., R.M. Menges, and P.R. Nixon. 1985. Distinguishing weed from crop plants using video remote sensing. Photogrammetric Engineering and Remote Sensing 51(11):1785-1790.

Scherz, J.P., and J.F.V. Domelen. 1975. Water quality indicators obtainable from aircraft and landsat images and their use in classifying lakes, p. 447-460. In Proceedings of the tenth international symposium on remote sensing of environment, Environment Research Institure of Michigan, Ann Arbor, Michigan.

Schowengerdt, R.A. 1983. Techniques for image processing and classification in remote sensing. Academic Press, Inc., New York. 249 p.

Swain, P.H., and S.M. Davis (Eds). 1978. Remote sensing: the quantitative approach. McGraw-Hill International Book Company, New York. 396 p.

Tiner, R.W., Jr. 1990. Use of high-altitude aerial photography for inventorying forested wetlands in the United States. Forest Ecology and Management 33/34:593-604.

Want, W.L. 1989. Law of wetlands regulation. Clark Boardman, New York. 1032 p.

Wolf, P.R., and R.C. Brinker. 1989. Elementary surveying. Eighth edition. Harper & Row, Publishers, New York. 696 p.

Yuan, X., D. King, and J. Vlcek. 1991. Sugar maple decline assessment based on spectral and textural analysis of multispectral aerial videography. Remote Sensing of the Environment 37:47-54.

APPENDIXES

Appendix A

Signature Separability Listing for Figure 6

File: w1g-test
Distance measure: Transformed Divergence
Using bands: 123
Taken 3 at a time

Class	(Weight)/(TotalWeight)
1. Veg-2	.071
2. Veg-3	.071
3. Veg-5	.071
4. Veg-6	.071
5. Veg-7	.071
6. Veg-8	.071
7. Veg-9	.071
8. Veg-10	.071
9. Veg-11	.071
10. Veg-12	.071
11. Grnd-1	.071
12. Water-1	.071
13. Water-2	.071
14. Veg-13	.071

Separability Listing

Bands	AVE	MIN	Class Pairs:						
			1:2	1:3	1:4	1:5	1:6	1:7	1:8
			1:9	1:10	1:11	1:12	1:13	1:14	2:3
			2:4	2:5	2:6	2:7	2:8	2:9	2:10
			2:11	2:12	2:13	2:14	3:4	3:5	3:6
			3:7	3:8	3:9	3:10	3:11	3:12	3:13
			3:14	4:5	4:6	4:7	4:8	4:9	4:10
			4:11	4:12	4:13	4:14	5:6	5:7	5:8
			5:9	5:10	5:11	5:12	5:13	5:14	6:7
			6:8	6:9	6:10	6:11	6:12	6:13	6:14
			7:8	7:9	7:10	7:11	7:12	7:13	7:14
			8:9	8:10	8:11	8:12	8:13	8:14	9:10
			9:11	9:12	9:13	9:14	10:11	10:12	10:13
			10:14	11:12	11:13	11:14	12:13	12:14	13:14
1 2 3	1985	1531	2000	2000	2000	2000	2000	2000	2000
			2000	2000	2000	2000	2000	2000	2000

2000	2000	1932	2000	2000	2000	2000
2000	2000	2000	2000	2000	2000	2000
2000	2000	2000	2000	2000	2000	2000
2000	1893	2000	2000	1856	1913	2000
2000	2000	2000	2000	2000	2000	1983
1810	2000	2000	2000	2000	2000	2000
2000	2000	2000	2000	2000	2000	2000
2000	2000	2000	1755	2000	2000	2000
1531	2000	2000	2000	2000	2000	2000
2000	2000	2000	2000	2000	2000	2000
1996	2000	2000	2000	1994	2000	2000

Appendix B

Signature Separability Listing for Figure 7

File: w1j-test
Distance measure: Transformed Divergence
Using bands: 123
Taken 3 at a time

Class	(Weight)/(TotalWeight)
1. Veg-1	.045
2. Veg-2	.045
3. Veg-3	.045
4. Veg-6	.045
5. Veg-7	.045
6. Veg-8	.045
7. Veg-9	.045
8. Veg-10	.045
9. Veg-11	.045
10. Veg-12	.045
11. Veg-13	.045
12. Veg-14	.045
13. Veg-15	.045
14. Veg-16	.045
15. Grnd-1	.045
16. Grnd-3	.045
17. Road-1	.045
18. Road-2	.045
19. Water-1	.045
20. Water-2	.045
21. Shadow-1	.045
22. Shadow-2	.045

Separability Listing

Bands	AVE	MIN	Class Pairs:						
			1:2	1:3	1:4	1:5	1:6	1:7	1:8
			1:9	1:10	1:11	1:12	1:13	1:14	1:15
			1:16	1:17	1:18	1:19	1:20	1:21	1:22
			2:3	2:4	2:5	2:6	2:7	2:8	2:9
			2:10	2:11	2:12	2:13	2:14	2:15	2:16
			2:17	2:18	2:19	2:20	2:21	2:22	3:4

			3:5	3:6	3:7	3:8	3:9	3:10	3:11
			3:12	3:13	3:14	3:15	3:16	3:17	3:18
			3:19	3:20	3:21	3:22	4:5	4:6	4:7
			4:8	4:9	4:10	4:11	4:12	4:13	4:14
			4:15	4:16	4:17	4:18	4:19	4:20	4:21
			4:22	5:6	5:7	5:8	5:9	5:10	5:11
			5:12	5:13	5:14	5:15	5:16	5:17	5:18
			5:19	5:20	5:21	5:22	6:7	6:8	6:9
			6:10	6:11	6:12	6:13	6:14	6:15	6:16
			6:17	6:18	6:19	6:20	6:21	6:22	7:8
			7:9	7:10	7:11	7:12	7:13	7:14	7:15
			7:16	7:17	7:18	7:19	7:20	7:21	7:22
			8:9	8:10	8:11	8:12	8:13	8:14	8:15
			8:16	8:17	8:18	8:19	8:20	8:21	8:22
			9:10	9:11	9:12	9:13	9:14	9:15	9:16
			9:17	9:18	9:19	9:20	9:21	9:22	10:11
			10:12	10:13	10:14	10:15	10:16	10:17	10:18
			10:19	10:20	10:21	10:22	11:12	11:13	11:14
			11:15	11:16	11:17	11:18	11:19	11:20	11:21
			11:22	12:13	12:14	12:15	12:16	12:17	12:18
			12:19	12:20	12:21	12:22	13:14	13:15	13:16
			13:17	13:18	13:19	13:20	13:21	13:22	14:15
			14:16	14:17	14:18	14:19	14:20	14:21	14:22
			15:16	15:17	15:18	15:19	15:20	15:21	15:22
			16:17	16:18	16:19	16:20	16:21	16:22	17:18
			17:19	17:20	17:21	17:22	18:19	18:20	18:21
			18:22	19:20	19:21	19:22	20:21	20:22	21:22
1 2 3	1994	1228	2000	2000	2000	2000	2000	2000	2000
			2000	2000	2000	2000	2000	2000	2000
			2000	2000	2000	2000	2000	2000	2000
			2000	2000	2000	2000	2000	2000	2000
			2000	2000	2000	2000	2000	2000	2000
			2000	2000	2000	2000	2000	2000	2000
			2000	2000	2000	2000	2000	2000	2000
			2000	2000	2000	2000	2000	2000	2000
			2000	2000	2000	2000	2000	2000	2000
			2000	2000	2000	2000	2000	2000	2000
			2000	2000	2000	2000	2000	2000	2000
			2000	2000	2000	2000	2000	2000	2000
			2000	2000	2000	2000	2000	2000	2000
			2000	2000	2000	2000	2000	2000	2000
			2000	1990	2000	2000	2000	2000	2000
			2000	2000	2000	2000	2000	2000	2000
			2000	2000	2000	1996	2000	2000	2000

2000	2000	2000	2000	2000	2000	2000
1999	2000	2000	1991	2000	1228	2000
2000	2000	2000	2000	2000	2000	2000
1646	2000	1992	2000	2000	2000	2000
2000	2000	2000	2000	2000	2000	2000
1997	1906	2000	2000	2000	2000	2000
2000	2000	2000	2000	2000	2000	2000
2000	2000	2000	2000	2000	2000	2000
2000	2000	2000	2000	2000	2000	2000
2000	2000	2000	2000	2000	2000	2000
2000	2000	2000	2000	2000	2000	2000
2000	2000	2000	2000	2000	2000	2000
2000	2000	2000	2000	2000	2000	2000
2000	1948	2000	2000	2000	2000	2000
2000	2000	2000	2000	2000	2000	2000
2000	2000	2000	2000	2000	2000	1999

Appendix C

Signature Separability Listing for Figure 8

File:w2h-test
Distancemeasure:TransformedDivergence
Usingbands:123
Taken3atatime

Class	(Weight)/(TotalWeight)
1. Veg-1	.059
2. Veg-3	.059
3. Veg-4	.059
4. Veg-7	.059
5. Veg-8	.059
6. Veg-9	.059
7. Veg-10	.059
8. Veg-11	.059
9. Veg-12	.059
10. Veg-13	.059
11. Veg-14	.059
12. Grnd-1	.059
13. Grnd-2	.059
14. Road-1	.059
15. Road-2	.059
16. Road-3	.059
17. Shadow-1	.059

SeparabilityListing

Bands	AVE	MIN	ClassPairs:						
			1:2	1:3	1:4	1:5	1:6	1:7	1:8
			1:9	1:10	1:11	1:12	1:13	1:14	1:15
			1:16	1:17	2:3	2:4	2:5	2:6	2:7
			2:8	2:9	2:10	2:11	2:12	2:13	2:14
			2:15	2:16	2:17	3:4	3:5	3:6	3:7
			3:8	3:9	3:10	3:11	3:12	3:13	3:14
			3:15	3:16	3:17	4:5	4:6	4:7	4:8
			4:9	4:10	4:11	4:12	4:13	4:14	4:15
			4:16	4:17	5:6	5:7	5:8	5:9	5:10
			5:11	5:12	5:13	5:14	5:15	5:16	5:17
			6:7	6:8	6:9	6:10	6:11	6:12	6:13
			6:14	6:15	6:16	6:17	7:8	7:9	7:10

			7:11	7:12	7:13	7:14	7:15	7:16	7:17
			8:9	8:10	8:11	8:12	8:13	8:14	8:15
			8:16	8:17	9:10	9:11	9:12	9:13	9:14
			9:15	9:16	9:17	10:11	10:12	10:13	10:14
			10:15	10:16	10:17	11:12	11:13	11:14	11:15
			11:16	11:17	12:13	12:14	12:15	12:16	12:17
			13:14	13:15	13:16	13:17	14:15	14:16	14:17
			15:16	15:17	16:17				
1 2 3	1984	1298	2000	2000	2000	2000	2000	2000	2000
			2000	2000	2000	2000	2000	2000	2000
			2000	2000	2000	2000	2000	2000	2000
			2000	2000	2000	2000	2000	2000	2000
			2000	2000	2000	2000	2000	2000	2000
			2000	2000	2000	2000	2000	2000	2000
			2000	2000	2000	2000	2000	2000	1978
			2000	2000	2000	2000	2000	2000	2000
			2000	2000	2000	2000	2000	2000	2000
			2000	2000	2000	2000	2000	2000	2000
			2000	2000	2000	2000	2000	2000	2000
			2000	2000	2000	2000	2000	1999	1970
			1915	2000	2000	2000	2000	2000	2000
			2000	2000	2000	2000	2000	2000	2000
			2000	2000	1298	1923	2000	2000	2000
			2000	2000	2000	1399	2000	2000	2000
			2000	2000	2000	2000	2000	2000	2000
			2000	2000	1507	2000	2000	2000	2000
			2000	2000	2000	2000	2000	1908	2000
			1994	2000	2000				

Appendix D

Black and white copies of color prints

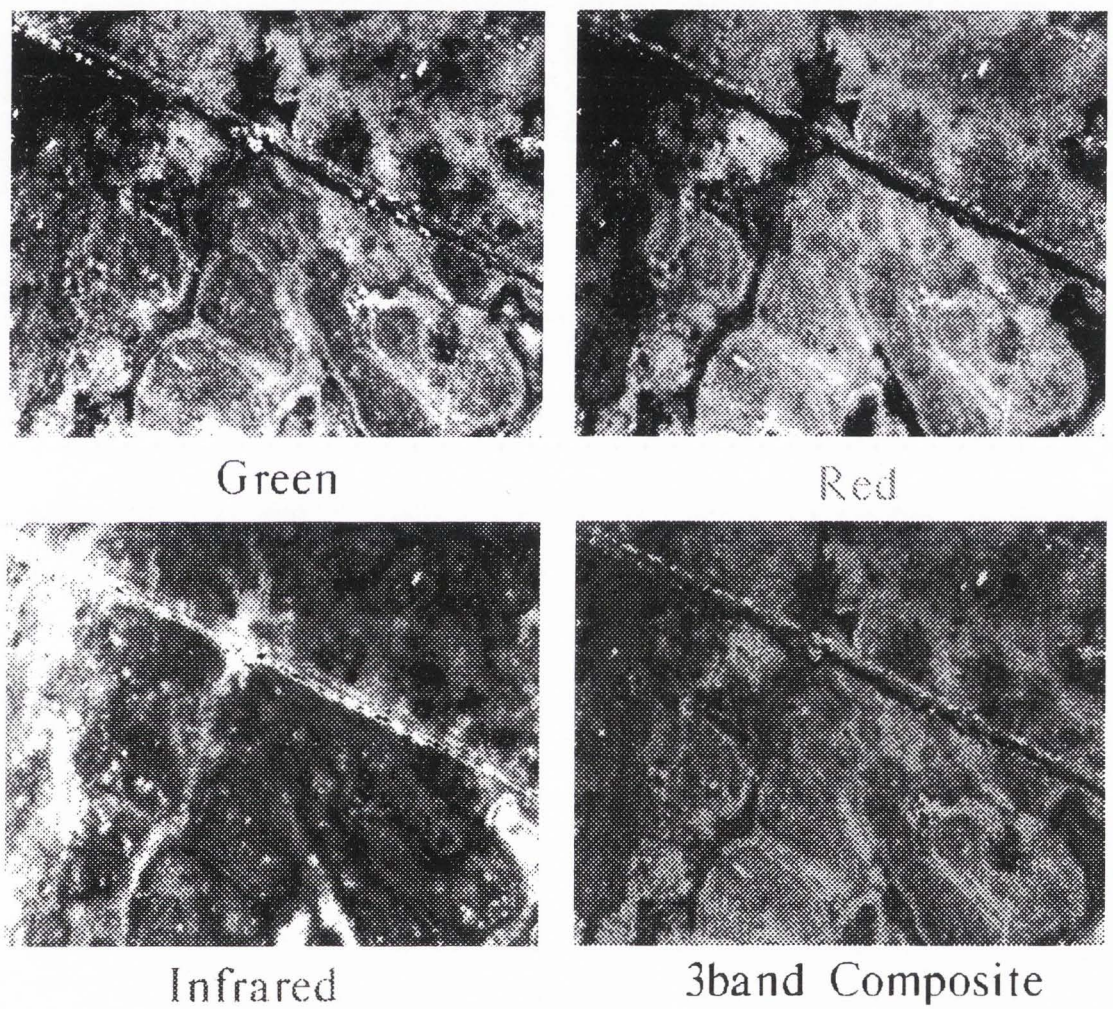

Figure 2. Example Single Bands and 3-band False Color Composite

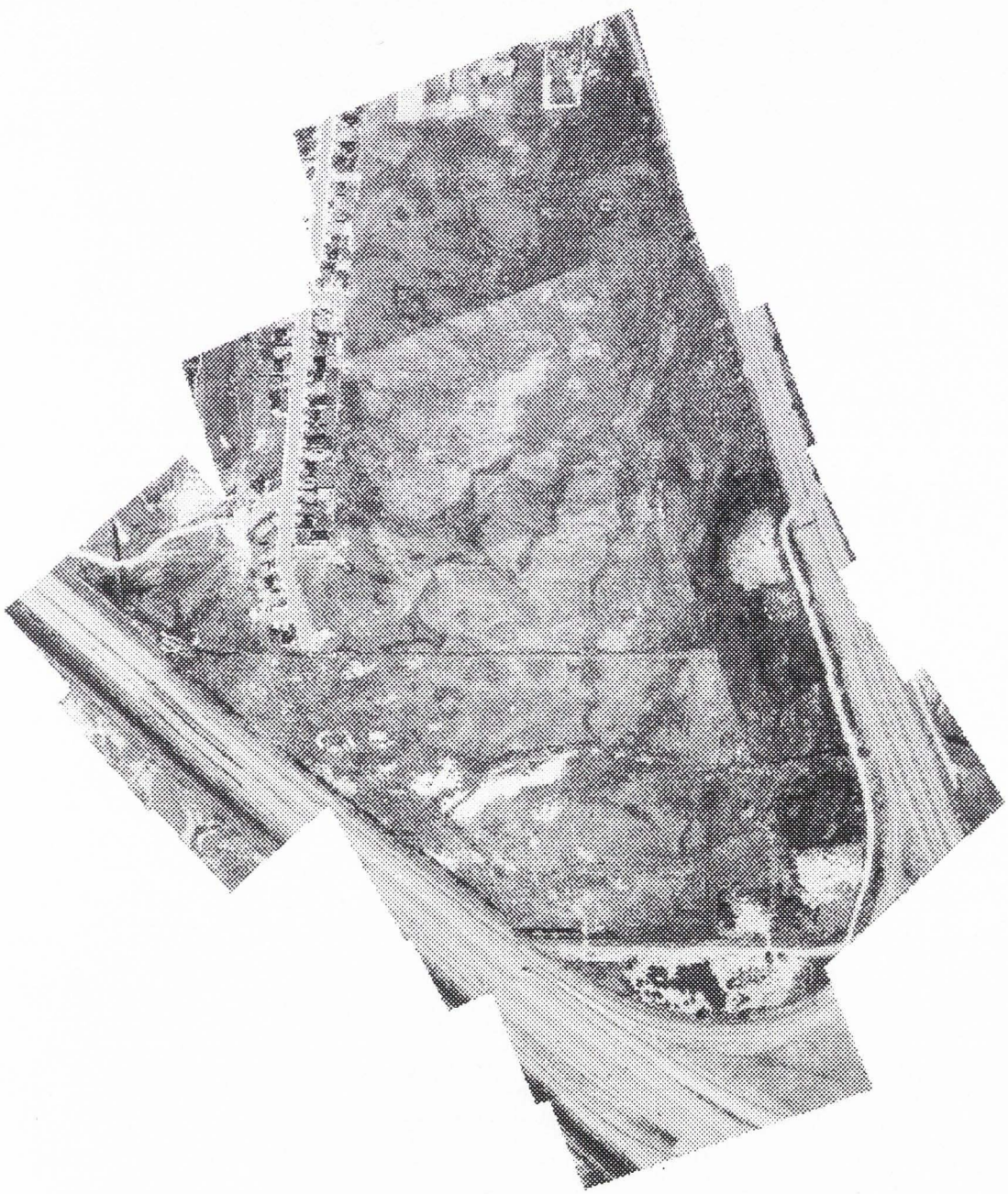

Figure 3. June 2, 1992 mosaic image

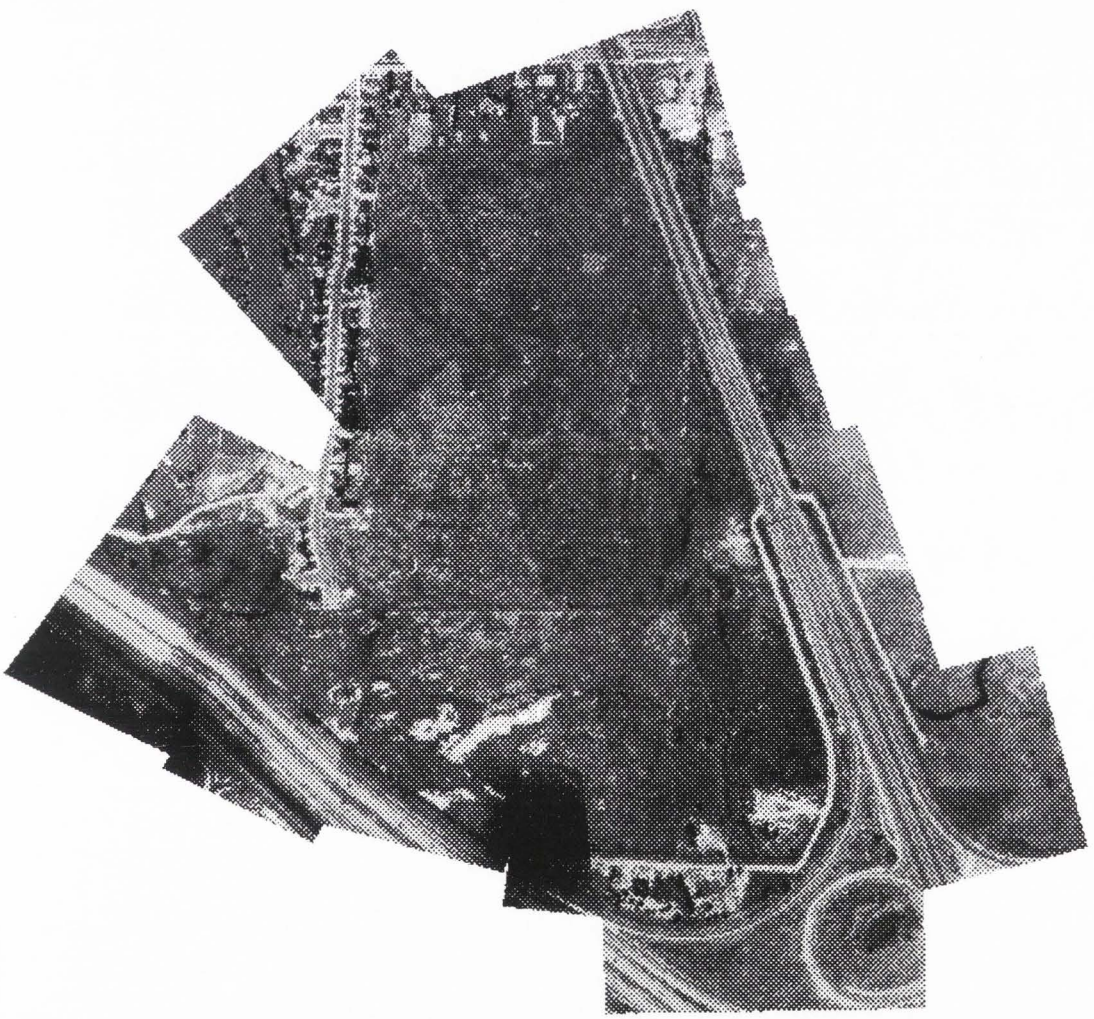

Figure 4. July 22, 1992 mosaic image

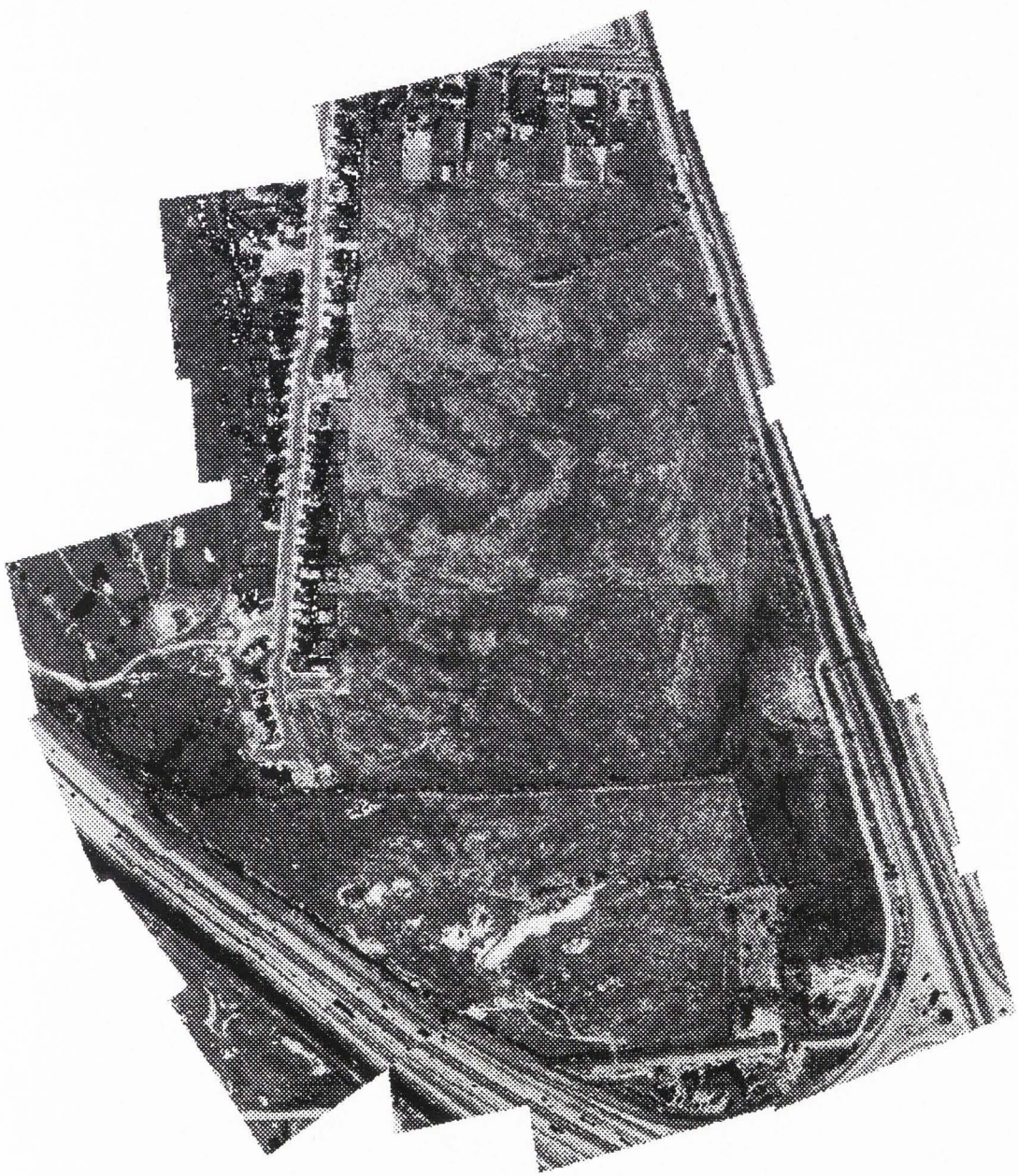

Figure 5. October 1, 1992 mosaic image

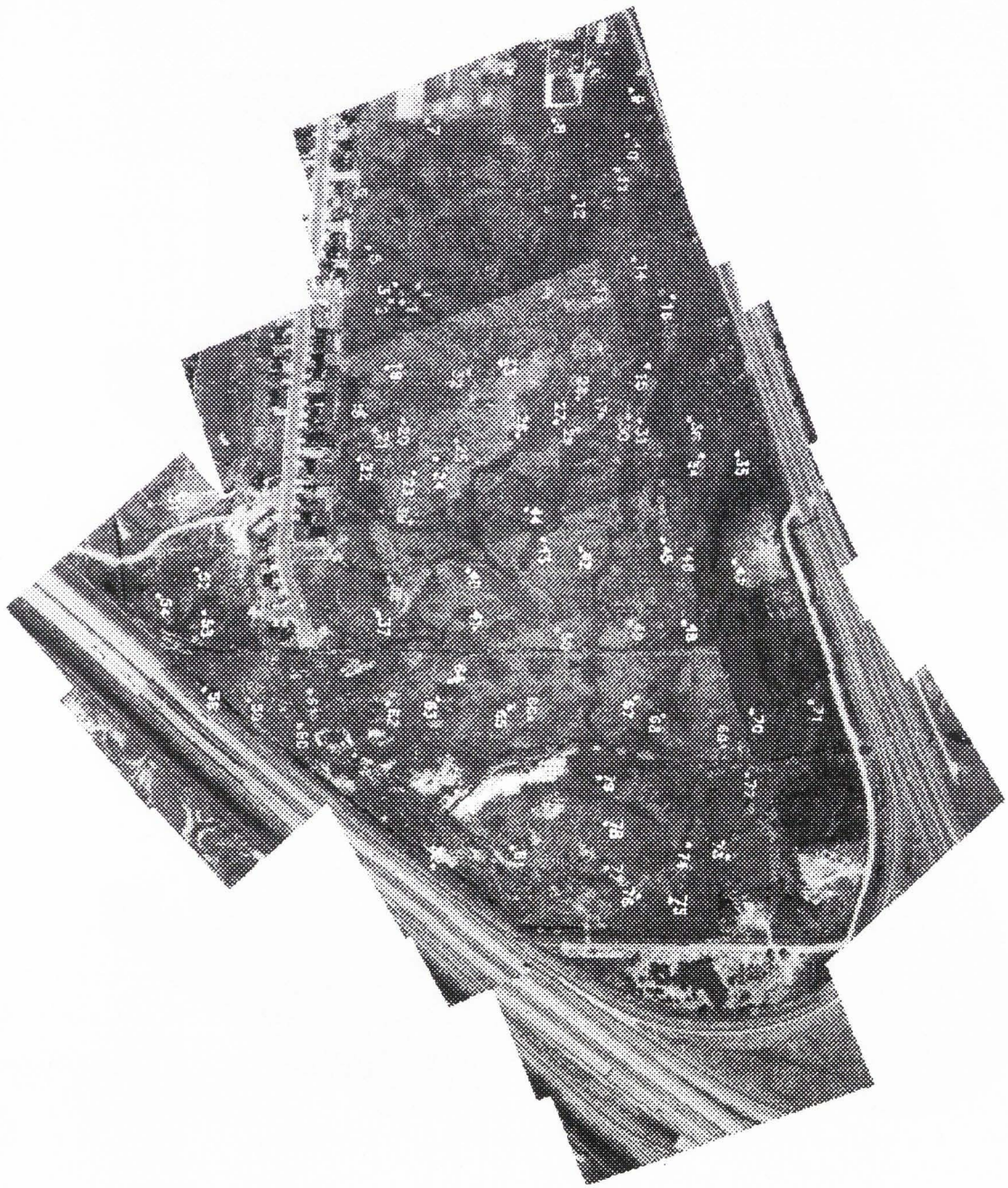

Figure 9. Location of ground based sample points divided into training set (yellow points) and verification set (white points)

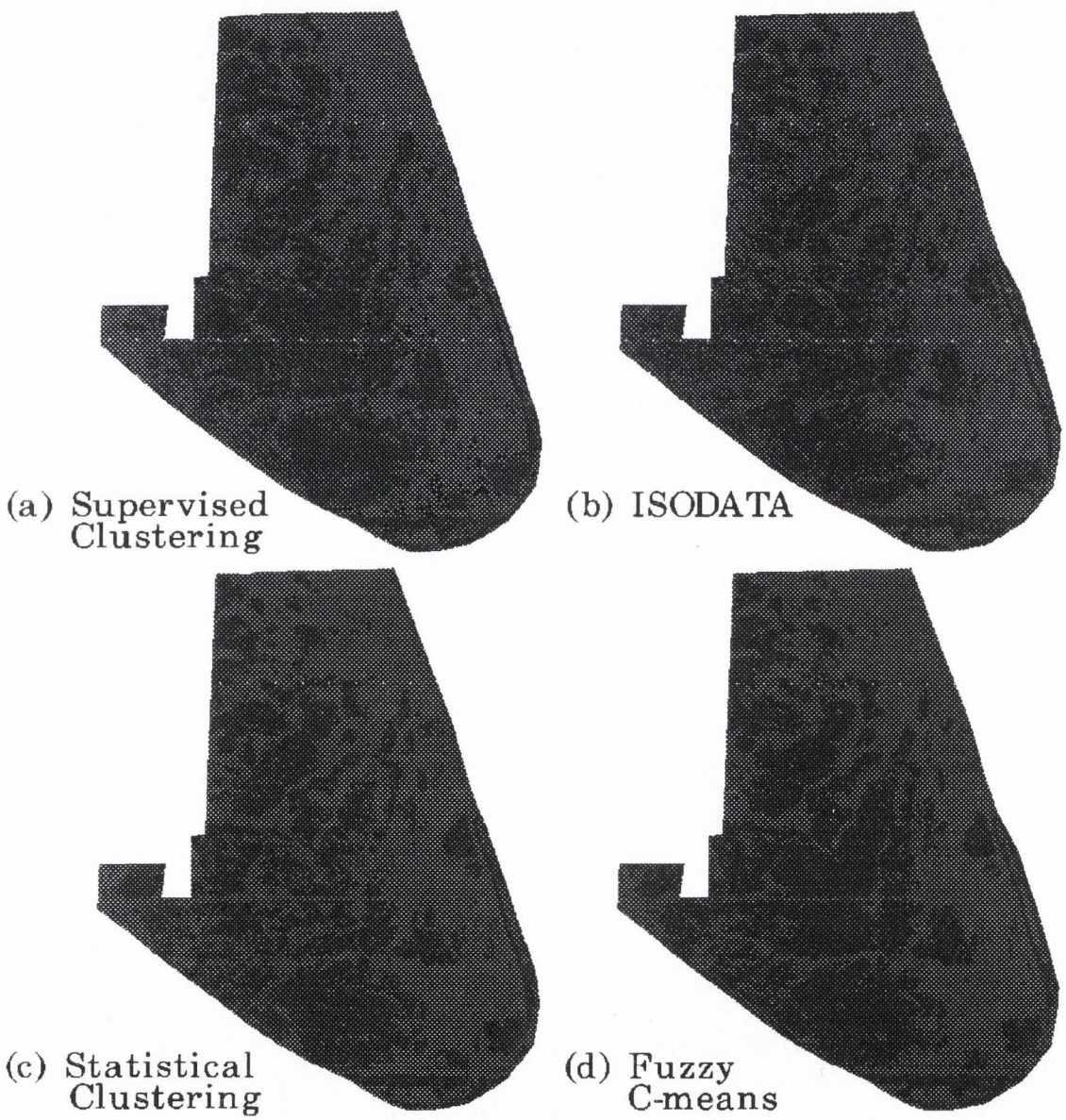

Figure 10. June 2, 1992 classified imagery

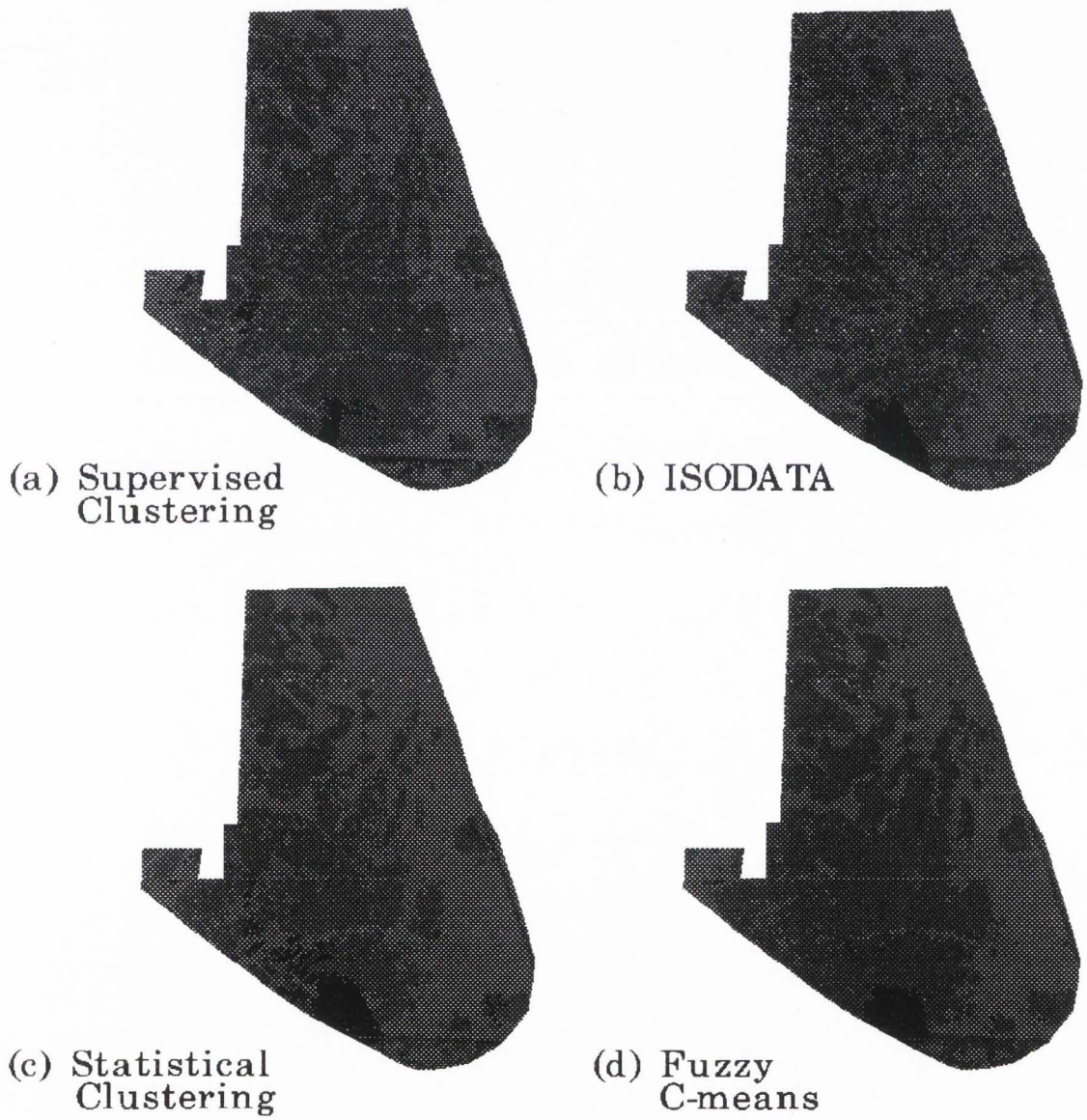

Figure 11. July 22, 1992 classified imagery

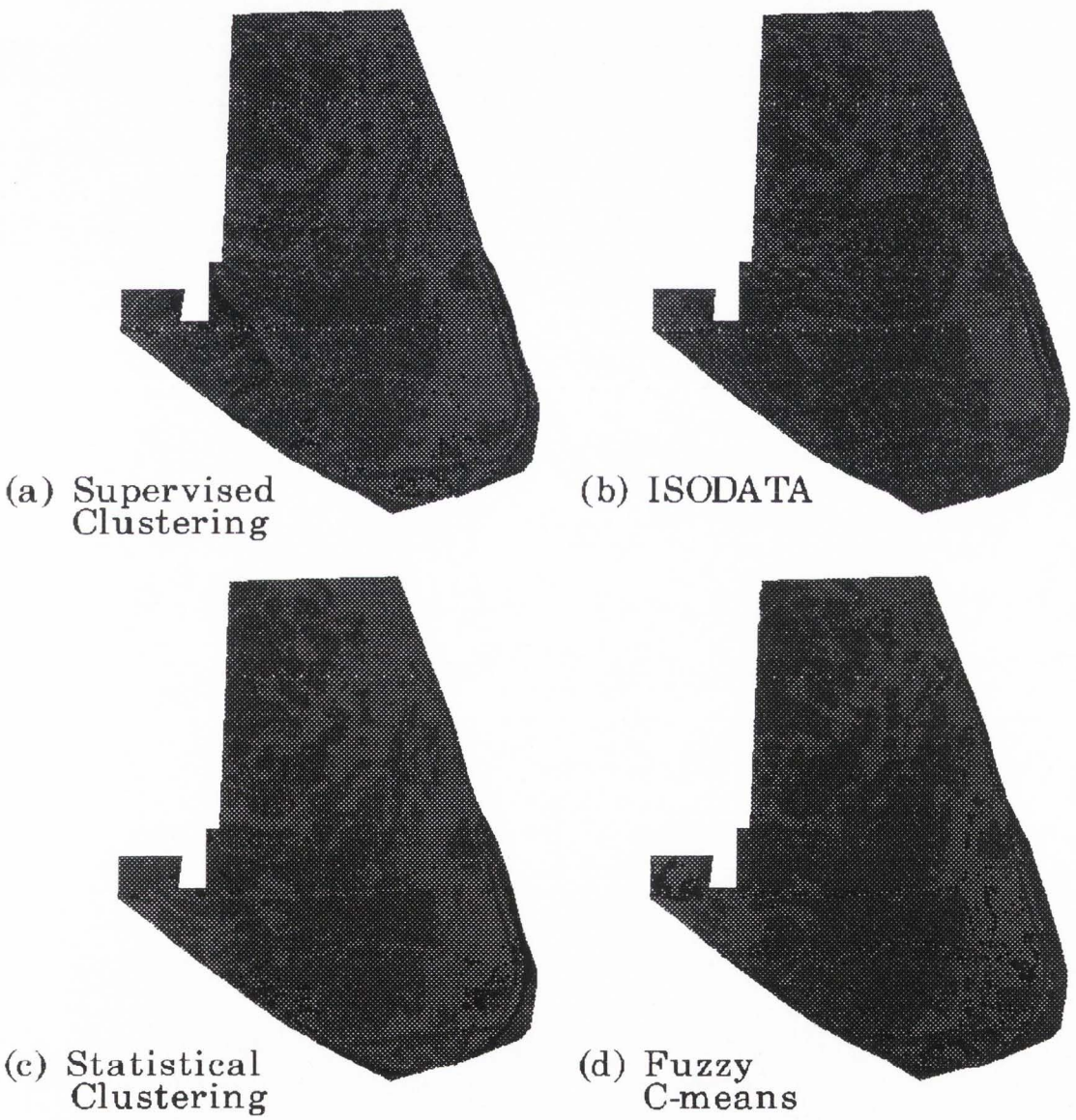

Figure 12. October 1, 1992 classified imagery

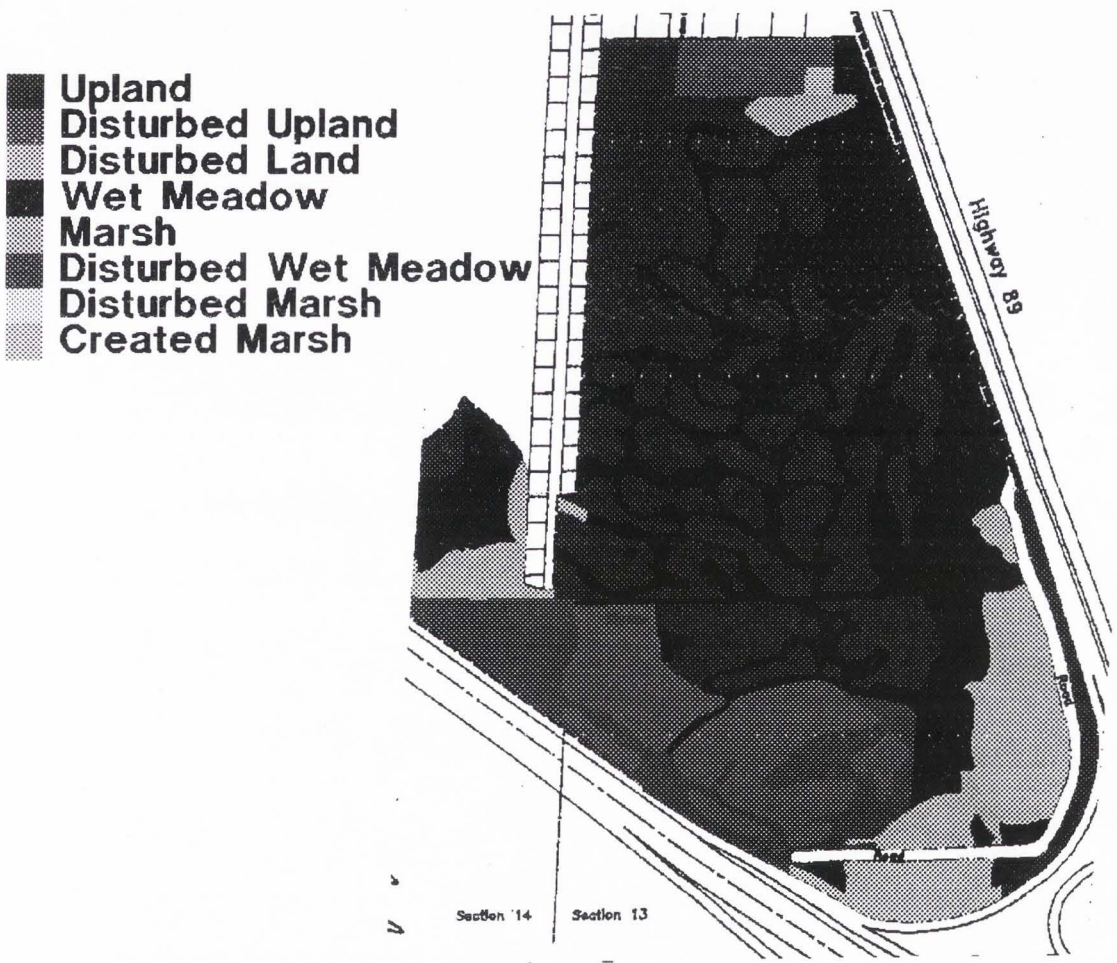

Figure 13. Ground truth map from original juridictional delineation

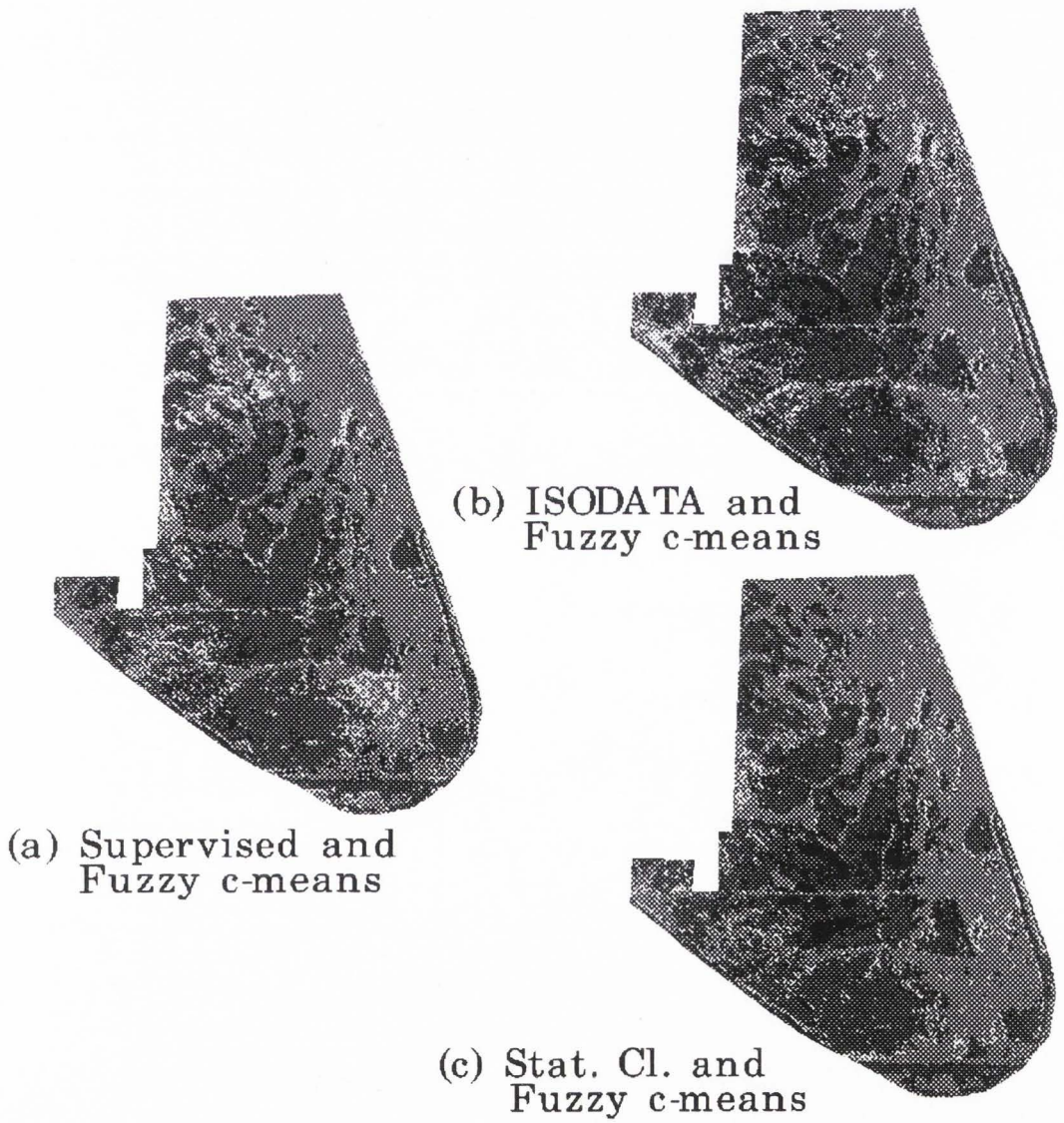

Figure 19. June flight date Fuzzy c-means overlaid on all three parametric techniques. (Dk gray - upland/both; Lt Gray - wetland/both; Blue - upland/Fuzzy, wetland/parametric; Yellow - wetland/Fuzzy, upland/parametric)